# Characterization of biogenic volatile organic compounds and their oxidation products at a stressed spruce-dominated forest close to a biogas power plant

Junwei Song[1,4,*], Georgios I. Gkatzelis[2], Ralf Tillmann[2], Nicolas Brüggemann[3], Thomas Leisner[1] and Harald Saathoff[1,*]

[1] Institute of Meteorology and Climate Research, Karlsruhe Institute of Technology, Hermann-von-Helmholtz-Platz 1, 76344 Eggenstein-Leopoldshafen, Germany

[2] Institute of Energy and Climate Research, IEK-8: Troposphere, Forschungszentrum Jülich GmbH, 52425 Jülich, Germany

[3] Institute of Bio- and Geosciences, IBG-3: Agrosphere, Forschungszentrum Jülich GmbH, 52425 Jülich, Germany

[4] Université Claude Bernard Lyon 1, CNRS, IRCELYON, UMR 5256, F-69626, Villeurbanne, France

Correspondence: Junwei Song (junwei.song@ircelyon.univ-lyon1.fr) and Harald Saathoff (harald.saathoff@kit.edu)

**Abstract**

Biogenic volatile organic compounds (BVOCs) are key components of the atmosphere, playing a significant role in the formation of organic aerosols (OA). However, only few studies have simultaneously examined the characteristics of BVOCs and OA in the forest under the impact of consecutive droughts and extensive bark beetle infestations. Here we present real-time measurements of OA and BVOCs at a stressed Norway spruce-dominated forest near a biogas power plant (BPP) in western Germany during June 2020. A proton-transfer-reaction time-of-flight mass spectrometer coupled with a particle inlet (CHARON-PTR-ToF-MS) and a Vocus-PTR-ToF-MS were used to measure OA and BVOCs. The average mass concentration of OA was $0.8 \pm 0.5$ µg m$^{-3}$, consisting mainly of semi-volatile monoterpene oxidation products. The average mixing ratios of isoprene ($0.58 \pm 0.54$ ppb) and monoterpenes ($2.5 \pm 5.3$ ppb) were higher than the values previously measured in both German temperate forests and boreal forests. Based on wind direction analysis, BVOC data were categorized into two groups with one mainly influenced by the biogenic emissions from an intact forest and a clear-cut area (biogenic-group) and another one by the anthropogenic emissions from a BPP and a village (anthropogenic-group). High mixing ratios of monoterpenes were observed in the anthropogenic-group, indicating a significant contribution of BPP emissions. In the biogenic-group, the variations of BVOC mixing ratios were driven by the interplay between meteorology, biogenic emissions and their photochemical consumption. Positive matrix factorization analysis of VOCs revealed substantial contributions of oxygenated organic compounds from the photochemical oxidation of BVOCs during daytime, while monoterpenes and their weakly oxidized products dominated at night. Furthermore, increasing relative humidity and decreasing temperatures promoted the gas-to-particle partitioning of these weakly oxidized monoterpene products, leading to an increase in nighttime OA mass. The results demonstrate the variations of BVOCs are influenced not only by meteorological conditions and biogenic emissions but also by local BPP emissions and subsequent chemical transformation processes. This study highlights the need to investigate the changes of biogenic emissions in European stressed forests.

# 1 Introduction

Volatile organic compounds (VOCs) play important roles in determining atmospheric chemical processes (Atkinson, 2000; Hallquist et al., 2009; Yáñez-Serrano et al., 2020; Shrivastava et al., 2017; Rasmussen and Went, 1965; Trainer et al., 1987; Peñuelas and Staudt,

51  2010). Terrestrial ecosystems emit large amounts of biogenic VOCs (BVOCs, >1000 Tg yr$^{-1}$)

52  to the global atmosphere, more than anthropogenic VOCs (AVOCs, ~200 Tg yr$^{-1}$) (Guenther et

53  al., 2012; Sindelarova et al., 2014). BVOCs emitted by vegetation consist largely of reactive

54  terpenoids e.g., isoprene (~70%), monoterpenes (~11%) and sesquiterpenes (~2.5%)

55  (Sindelarova et al., 2014). The oxidation products of terpenoids can nucleate to form new

56  particles or contribute to the growth of existing particles and secondary organic aerosol (SOA)

57  formation, thus impacting air quality and climate (Hallquist et al., 2009; Shrivastava et al.,

58  2017).

59      Over the last decade, many field studies have been conducted at different forest ecosystems

60  to investigate the characteristics of BVOCs including the emissions, temporal variations as well

61  as their impacts on atmospheric reactivity and SOA formation (Hakola et al., 2012; Hellén et

62  al., 2018; Li et al., 2020; Huang et al., 2021; Yáñez-Serrano et al., 2021; Vestenius et al., 2021;

63  Mermet et al., 2021; Vermeuel et al., 2023; Weber et al., 2022; Bourtsoukidis et al., 2024;

64  Bourtsoukidis et al., 2014). The diurnal pattern of isoprene concentrations in forests shows

65  typically higher values during daytime (Yáñez-Serrano et al., 2021; Li et al., 2020; Hakola et

66  al., 2012), since isoprene emissions increase with temperature and sunlight intensity as result

67  of increased de-novo production and direct release. In contrast, monoterpenes are mainly

68  released from storage pools of boreal pines. The emissions and composition of BVOCs from

69  trees varies with abiotic and biotic stresses such as high temperature (Teskey et al., 2015; Kleist

70  et al., 2012), drought (Peron et al., 2021; Bonn et al., 2019) and herbivore attack (Jaakkola et

71  al., 2023; Kari et al., 2019; Faiola and Taipale, 2020). It has been reported that these stresses

72  can alter the emissions of BVOCs, especially of terpenoids (Ghimire et al., 2016; Jaakkola et

73  al., 2023; Byron et al., 2022).

74      In addition to biogenic emissions, the temporal variations of BVOC concentrations

75  especially of terpenoids are influenced by atmospheric oxidation processes. The diurnal

76  variation of monoterpene concentrations shows lower values during daytime than nighttime in

77  the boreal forests, which were attributed to the rapid photochemical consumption and expanded

78  boundary layer heights (Hellén et al., 2018; Hakola et al., 2012). Correspondingly, higher

79  concentrations of monoterpene oxidation products are expected to be produced during daytime.

80  For instance, Huang et al., (2021) found that some gaseous monoterpene oxidation products

81  e.g., $C_7H_{10}O_4$ (3,6-oxoheptanoic acid) and $C_8H_{12}O_4$ (terpenylic acid) showed higher

82  concentrations during daytime in a boreal forest. Li et at., (2020) reported similar diurnal

83  variations of gaseous higher-oxidized monoterpene products (e.g., $C_8H_{12}O_{4-6}$, $C_9H_{14}O_{4-6}$,

84  $C_{10}H_{14}O_{4-6}$ and $C_{10}H_{16}O_{4-6}$) in the French Landes-forest largely composed of maritime pines.

85    The variations of BVOC oxidation products are also influenced by gas-particle partitioning
86    processes. Laboratory studies have shown that decreasing temperature and increasing relative
87    humidity (RH) can lead to an increased particulate fraction of SOA products from BVOC
88    oxidation (Surdu et al., 2023; Von Hessberg et al., 2009; Tillmann et al., 2010; Zhang et al.,
89    2015; Luo et al., 2024). However, due to lack of online dual-phase measurements only few field
90    studies have focused on the gas-particle partitioning of BVOC oxidation products in the healthy
91    forests (Mohr et al., 2017; Yatavelli et al., 2014; Isaacman-Vanwertz et al., 2016; Lee et al.,
92    2018). However, our understanding of the interplay between gas and particle phases of BVOC
93    oxidation products in real forest atmosphere, particularly in stressed forest, remains limited.
94    Addressing these gaps is crucial for assessing the impact of various environmental factors on
95    BVOC emissions and their subsequent transformation (Faiola and Taipale, 2020).

96    The Eifel is a low mountain range in western Germany that stretches across the federal states
97    of North Rhine-Westphalia and Rhineland-Palatinate and covers an area of ~5300 km$^2$. Its
98    forested areas are largely composed of Norway spruce (*Picea abies* (L.) Karst.), which are
99    important contributors to BVOCs (Smiatek and Steinbrecher, 2006; Kleist et al., 2012). The
100   Eifel Forest was suffering from severe droughts, heatwaves and bark beetle infestation in the
101   years before our measurements, thus it can serve as a case for examining the variations of
102   BVOCs in a stressed European coniferous forest. In this study, a field measurement campaign
103   was conducted at a site of the northern Eifel Forest in the vicinity of a biogas power plant (BPP).
104   Europe is the world leader in biogas electricity production with more than 18,000 BPPs
105   (Brémond et al., 2021). These BPPs are widely distributed in European rural areas close to the
106   forest region (Bakkaloglu et al., 2021; Scheftelowitz et al., 2018), which emit large amounts of
107   CH$_4$ and VOCs periodically to the atmosphere around the BPPs (Salazar Gómez et al., 2016).
108   In this paper, we present the real-time measurements of VOCs and aerosol particles measured
109   by a proton-transfer-reaction time-of-flight mass spectrometer (PTR-ToF-MS) coupled with a
110   particle inlet (CHARON, chemical analysis of aerosol online) and a Vocus-PTR-ToF-MS. The
111   impacts of meteorological conditions, sources and chemical oxidation processes on the
112   variations of BVOCs and their gaseous and particulate oxidation products were investigated to
113   get a better understanding of BVOC emissions and their contributions to SOA as well as the
114   potential impact of BPP emissions.

## 2 Methods

### 2.1 Sampling site

In In this study, a three-week field campaign was conducted at a site in the northern Eifel Forest (50.72° N, 6.40° E) during June 2020 as a part of the "Heat and Drought 2020" campaign of the Modular Observation Solutions of Earth Systems (MOSES) project of the Helmholtz Association of German Research Centers. The Eifel Forest was suffering from severe droughts, heatwaves and severe bark beetle infestation in the last years (Weber et al., 2022b; Ghimire et al., 2016). Within two years (2018-2020), 14% of the spruce in the Northern Eifel region were removed due to summer droughts and only 28.3% remained in good condition (Montzka et al., 2021). Therefore, the Eifel Forest can serve as an example of a stressed temperate coniferous forest.

As shown in **Fig. 1**, the measurement site is situated directly next to a stand of Norway spruce with a few shrubs and blueberry plants also surrounding the area. To the south and southeast of the measurements site, there were some clear-cut areas due to bark beetle infestation in the years of 2018-2020. Additionally, the measurement site was located ~400 m southeast of a football field in the small village Kleinhau belonging to the municipality of Hürtgenwald, Germany (population about 9000) and ~250 m east of a BPP (BioEnergie Kleinhau GmbH). The biomass substrate used for the biogas production in this BPP consisted mainly of crop waste (e.g., corn stover). The measurement site was affected by the BPP emissions especially for westerly wind directions.

### 2.2 Instrumentation

All instruments were set up in a temperature-controlled measurement container (~25 °C) located at the sampling site. All sampling inlets were located 3.7 m above ground level and 1 m above the container roof. An overview of instruments and parameters measured is given in **Table S1**.

A PTR-ToF-MS 4000X2 coupled with a CHARON particle inlet (Ionicon Analytik GmbH, Innsbruck, Austria) was deployed to measure the VOCs and aerosol particles from $5^{th}$-$30^{th}$ of June 2020. A detailed description of the PTR-ToF-MS and CHARON inlet has been provided elsewhere (Jordan et al., 2009; Muller et al., 2017; Eichler et al., 2015). Briefly, CHARON consists of a charcoal denuder for stripping off gaseous organics, an aerodynamic lens for enriching particles, and a thermo-desorption unit for particle evaporation prior to chemical analysis by PTR-ToF-MS. In this campaign, both gases and particles were measured through alternatingly switching between different modes with the data acquisition software (IoniTOF

148 4.0, Ionicon Analytik GmbH, Innsbruck, Austria). Specifically, one alternating measurement

149 cycle includes 3-min HEPA filter mode for measuring the particle background, 1-min transition

150 mode for the instrument equilibrium, 10-min CHARON mode for measuring particle phase

151 compounds, another 1-min transition mode and 10-min VOC mode for measuring gas phase

152 compounds (**Fig. S1**). One minute transition time is sufficient for the equilibrium of

153 instrumental conditions between different modes (Piel et al., 2021). During the gas-phase

154 measurement, ambient air was sampled continuously from a 3 m long perfluoroalkoxy tube (1/4

155 inch inner diameter) with a total flowrate of 1.45 L min$^{-1}$, and then a subset flow of ~0.1 L min$^{-1}$

156 was sampled by the PTR-MS through a polyetheretherketone tubing maintained at 80 °C.

157 During the particle-phase measurement, ambient particles were sampled by a PM$_{2.5}$ inlet with a

158 flowrate of 16.7 L min$^{-1}$, out of which a flow of 0.55 L min$^{-1}$ was directed to the CHARON

159 inlet maintained by a vacuum pump (ACP15, Pfeiffer Vacuum). During a first measurement

160 stage from 5$^{th}$-19$^{th}$ of June, the PTR drift tube was set with alternating temperatures for gas and

161 particle phase measurement modes at 80 °C and 120 °C respectively. With this setting, the

162 actual drift tube temperatures were varying during the gas and particle measurement modes

163 complicating the data analysis (**Figs. S1 and S2**). During a second measurement stage from

164 22$^{nd}$-30$^{th}$ of June, the PTR drift tube was set with the same temperature of 120 °C and a drift

165 tube pressure of 2.7 mbar for both gas and particle measurement modes. The CHARON inlet

166 was set to a thermo-desorption unit temperature of 150 °C and a pressure of 7-8 mbar. Finally,

167 the electric field (E/N) of the CHARON-PTR-TOF-MS was kept at ~97 Td and ~57 Td for the

168 gas and particle phase measurement modes respectively during the second measurement stage.

169 Please note that during the first measurement stage the actual temperature of the drift tube

170 fluctuated and was lower than the intended temperature of 120 °C (**Fig. S1**). This made it

171 difficult to quantify organic compounds in the particle phase measured by the CHARON-PTR-

172 ToF-MS. For the gas phase measurements, we corrected the major VOC data from the first

173 measurement stage based on the gas calibration and the cross-comparison with Vocus-PTR-

174 ToF-MS measurements. Consequently, we can present the major VOC species measured by the

175 CHARON-PTR-ToF-MS for the entire campaign, while the particle phase data for first

176 measurement stage were excluded for further analysis in this study.

177 Gas calibrations of CHARON-PTR-TOF-MS were performed via dynamic dilution of a

178 calibration gas cylinder containing 11 VOC species (**Table S2**, accuracy 10% at ~100 ppb).

179 The background of VOCs was taken from zero-air measurements during the gas calibrations at

180 the beginning and the end of the campaign. The enrichment factor of the CHARON inlet was

181 determined using an external calibration with size-selected ammonium nitrate particles

182    ($NH_4NO_3$) that were counted using a condensation particle counter (CPC3772, TSI Inc.,

183    Shoreview, MN, USA). The enrichment factor was determined with an average value of $18 \pm 2$

184    in the 150-700 nm particle size range, with lower values for smaller particles below 150 nm

185    (**Fig. S3**). The particle background was determined by a high-efficiency HEPA filter (ETA filter

186    model HC01-5N-B, Aerocolloid LLC, Minneapolis, MN, USA) that was placed upstream of

187    the gas-phase denuder of the CHARON inlet. All data files recorded by the CHARON-PTR-

188    ToF-MS were processed by the software IONICON Data Analyzer (IDA version1.0.0.2,

189    Ionicon Analytik GmbH, Innsbruck, Austria). More details of data processing with the IDA are

190    given in **Supplement S1**.

191       A Vocus-PTR-ToF-MS (Aerodyne Research Inc., Billerica, MA, USA) was deployed to

192    measure VOCs and oxygenated VOCs concurrently with the CHARON-PTR-ToF-MS from

193    $10^{th}$-$30^{th}$ of June. The Vocus-PTR-ToF-MS was not available for measurements before $10^{th}$ June

194    2020 due to a technical problem. The details of the Vocus-PTR-ToF-MS have been described

195    elsewhere (Krechmer et al., 2018). The Vocus-PTR-ToF-MS is characterized by a newly

196    designed reagent-ion source and a focusing ion-molecule reactor (FIMR), both of which

197    improve the detection efficiency of ions. In this study, the FIMR was operated at a pressure of

198    1.5 mbar. The mass resolving power of the Vocus mass analyzer was ~10000 amu/Δamu. Raw

199    data were recorded with a time resolution of 5 s. For the Vocus-PTR-ToF-MS measurement,

200    ambient air was drawn in through a 1 m long PFA tubing with a total flow rate of 4.5 L min$^{-1}$,

201    and then a subset flow of 0.1-0.15 L min$^{-1}$ went into the Vocus-PTR-ToF-MS. Background

202    measurements using high-purity nitrogen were automatically performed every hour. The

203    Vocus-PTR-ToF-MS was regularly calibrated using a home-made gas standard of 15

204    compounds at ~1 ppmv with accuracy of 10% (**Table S2**). At the end of the campaign, a gas

205    cross calibration was performed between Vocus-PTR-ToF-MS and CHARON-PTR-ToF-MS

206    with the calibration gas cylinder (Ionicon Analytik GmbH). The Vocus-PTR-ToF-MS data

207    analysis was performed using the software package "TOFware" (AG, Thun, Switzerland). For

208    the quantification of uncalibrated species measured by the Vocus-PTR-ToF-MS, we adopted

209    the rate constants of proton transfer reactions ($K_{cap}$) from the PTR library (Pagonis et al., 2019).

210    We then generated a sensitivity for the uncalibrated masses by applying a correction factor

211    based on the $k_{cap}$ ratios to the calibrated masses. Finally, the Vocus-PTR-ToF-MS data were

212    synchronized to the measurement time of CHARON-PTR-ToF-MS for comparison of the VOC

213    data. In this study, a series of VOC species were simultaneously detected by the CHARON-

214    PTR-ToF-MS and the Vocus-PTR-ToF-MS with a detailed comparison provided in

215    **Supplement S2**.

In addition, methane ($CH_4$), carbon dioxide ($CO_2$), water vapor ($H_2O$) and carbon monoxide (CO) were measured with a cavity ring-down spectrometer (G2401; Picarro, Santa Clara, CA, USA) from $10^{th}$-$30^{th}$ of June. $O_3$ was measured by a commercial chemiluminescence analyzer (Cranox II, Eco Physics GmbH, Hürth, Germany). An optical particle counter (OPC, Fidas200, Palas, Karlsruhe, Germnay) was used to measure the mass concentrations of $PM_{2.5}$ and $PM_{10}$ from $5^{th}$-$30^{th}$ of June. Simultaneously, black carbon (BC) concentrations were measured with an aethalometer (MA200, AethLabs, CA, USA). Particle number concentrations were measured with a condensation particle counter (CPC3776, TSI Inc., Shoreview, MN, USA). A nanoparticle sizer (NanoScan SMPS, TSI3910, TSI Inc., Shoreview, MN, USA) was used to measure the particle number size distribution between 10-410 nm.

Meteorological parameters were measured by a compact sensor (WS700, Lufft GmbH, Fellbach, Germany). The meteorological data were missing during some short periods due to the malfunction of data acquisition. We also used hourly data of temperature, relative humidity (RH), precipitation, and planetary boundary layer (PBL) height from the European Centre for Medium-Range Weather Forecasts ERA5 reanalysis (Hersbach et al., 2020), as well as wind speed and direction data form NASA Power Data Access Viewer (power.larc.nasa.gov) to complement the meteorological data. The daily soil moisture was measured by a Cosmic-Ray Neutron Sensor (CRNS) (Bogena et al., 2015), which was located ~150 m southwest of the sampling site. In addition, the spatial distribution of soil moisture in the northern Eifel Forest was determined from the measurement of a CRNS rover.

**2.3 Positive matrix factorization analysis**

The PMF receptor model is a bilinear analytic algorithm that separates the time series of air pollutants to different sources represented by factor profiles, factor time series and residual signals (Paatero and Tapper, 1994). The PMF model has been widely used to determine different sources and chemical processes of VOCs measured by the PTR-ToF-MS in the urban, rural and forest atmospheres (Gkatzelis et al., 2021; Li et al., 2021a; Wang et al., 2020; Li et al., 2022; Pernov et al., 2021; Desservettaz et al., 2023; Jain et al., 2023; Song et al., 2024). To explore the sources and chemical processes of VOCs, we performed the PMF analysis of VOC species measured by the Vocus-PTR-ToF-MS rather than those measured by CHARON-PTR-ToF-MS. This is mainly due to the Vocus-PTR-ToF-MS can measure higher molecular weight OVOCs ($mz > 200$) well that provides more information for interpreting the oxidation processes of BVOCs (Li et al., 2021a).

In this study, the Vocus-PTR-ToF-MS-measured VOC ions with a chemical formula assignment (mainly $C_xH_y^+$ and $C_xH_yO_z^+$) were selected to perform the PMF analysis. The PMF input data was prepared according to the protocol reported in previous studies (Pernov et al., 2021; Li et al., 2022). The uncertainties were calculated with the following equations:

$$Unc. = \begin{cases} LOD \times \dfrac{5}{6} & conc \leq LOD \quad (1) \\ \sqrt{LOD^2 + (Error\ fraction \times conc.)^2} & conc. > LOD \quad (2) \end{cases}$$

where the concentrations of a VOC ion below the limit of detection (LOD) were replaced with half of the LOD and the associated uncertainties were set to 5/6 of the LOD using the Equation 1. The uncertainties of a VOC ion above the LOD were calculated using the Equation 2, assuming an error fraction of 10%. We excluded the VOC species from the PMF analysis if their concentration data are significantly below LOD (> 20%) during the entire measurement campaign. For example, we excluded the signal of $C_4H_9^+$ for PMF analysis because its signals were mostly below the LOD during a significant fraction of the measurement period (**Fig. S4**). Finally, 157 VOC ions were selected for the PMF analysis (**Table S3**). The sum mixing ratios of these 157 VOC ions measured by the Vocus-PTR-ToF-MS showed a good agreement with the sum mixing ratios of 112 major VOC ions simultaneously measured by the CHARON-PTR-ToF-MS (**Fig. S4**). Therefore, the solution of PMF analysis on these 157 VOC ions measured by the Vocus-PTR-ToF-MS can reasonably interpret the major sources and/or chemical processes of VOCs in this study. The PMF analysis was performed using the PMF Evaluation Tool (v3.05) that runs in IGOR Pro software (v6.37, Wavemetrics, Portland, OR). The optimal PMF solution was explored across several solution diagnostics of factors ranging 1 to 10. The 6-factor solution was chosen as the optimal and interpretable solution. After 6 factors, increasing the factor number will cause the factor splitting and provide uninterpretable results (**Fig. S5**). The summary of diagnostic plots for the 6-factor solution is given in **Fig. S6**.

**2.4 Calculation of particle-phase fraction of organic compounds**

To estimate the gas-to-particle partitioning processes, we calculated the particulate mass fraction ($F_p$) of organic compounds by the Equation 3:

$$F_p = \frac{C_{p,i}}{C_{g,i} + C_{p,i}} \tag{3}$$

where $C_{p,i}$ and $C_{g,i}$ are the particle and gas phase concentrations of the individual organic compound measured by CHARON-PTR-ToF-MS and Vocus-PTR-ToF-MS, respectively.

## 3 Results and discussion

In the first section we will give an overview of the measurements conducted and in the second section we will address the impacts of meteorological factors like wind speed and direction, temperature, and relative humidity on the variations of gas and particle concentrations. In the third section we perform a source apportionment of the VOCs observed, and in the last section we discuss BVOC oxidation products in gas and particle phase.

### 3.1 Overview of the measurements

### 3.1.1 Meteorology

During the entire measurement campaign, the ambient temperature ranged from 6.8 to 30.8 °C with an average of 16.6 ± 4.7 °C, and the relative humidity (RH) varied from 31% to 98% with an average of 71% ± 16% respectively (**Fig. 2**). The wind speeds ranged from 0-5.5 m s$^{-1}$ with an average of 1.3 ± 0.9 m s$^{-1}$. Wind directions varied significantly during the entire measurement period. The sampling site was potentially affected by BPP-related and/or anthropogenic emissions depending on the wind directions (**Fig. 1**). The leaf area index of the Eifel Forest during our measurement period was determined to be ~2.5 ± 0.02 m$^2$ m$^{-2}$ based on the ERA5 reanalysis data. The soil moisture was measured to be 0.3 ± 0.04 m$^3$ m$^{-3}$ at a station located ~150 m southwest of the sampling site. In addition, the spatial distribution of soil moisture in the northern Eifel Forest also showed low values (<0.3 m$^3$ m$^{-3}$) in most areas covering our sampling site (**Fig. S7**). Therefore, the Eifel Forest was under relatively dry condition during our measurement period.

During the entire measurement campaign, we observed two characteristic episodes, Episode 1 (0:00 9$^{th}$ of June to 0:00 12$^{th}$ of June) and Episode 2 (12:00 23$^{rd}$ of June to12:00 26$^{th}$ of June), for different meteorological conditions. During Episode 1, the daily maximum temperature remained below 20 ℃ for three consecutive measurement days. During Episode 2, the daily maximum temperature exceeded 25 ℃ for three consecutive measurement days. Therefore, hereafter we define these two episodes as low-T and high-T episodes, respectively. Both episodes had very low wind speeds (< 1 m s$^{-1}$), suggesting the site was influenced by local emissions and chemical transformation or aging processes. The impacts of meteorology and chemical processes on the variations of gases and particles will be discussed in the following sections.

### 3.1.2 Mixing ratios of gas species

As shown in **Fig. 3**, the average mixing ratios of CO and $CO_2$ were $0.11 \pm 0.02$ ppm and $410 \pm 1$ ppm respectively from $10^{th}$-$30^{th}$ of June. The mixing ratios of $CH_4$ ranged from 1.90 to 2.56 ppm with an average of $1.98 \pm 0.05$ ppm. Spikes of $CH_4$ (> 2.2 ppm) were occasionally observed during the days of 17, 20-21 and 23 June, which are associated with BPP-related emissions as validated in Section 3.2. Isoprene and monoterpenes were quantitatively measured by the CHARON-PTR-ToF-MS and Vocus-PTR-ToF-MS with good to fair correlations (r = 0.92 and 0.59 for isoprene and monoterpenes, respectively). During the entire campaign, the average mixing ratios of isoprene was $0.58 \pm 0.54$ ppb, slightly higher than that previously reported in a Norway spruce-dominated forest ($0.32 \pm 0.17$ ppb) in central Germany (Bourtsoukidis et al., 2014) and a mixed-conifer forest (max. 0.25 ppb) with Norway spruce and Scots pine (*Pinus sylvestris* L.) in Sweden (Petersen et al., 2023). The level of isoprene in this study was comparable to that (~0.6 ppb) observed in French Landes forest dominated by maritime pine trees (*Pinus pinaster* Aiton) during summer time (Li et al., 2020), but higher than those (0.01-0.2 ppb) reported for the boreal forests in Finland dominated by Scots pine (Li et al., 2021a; Hellén et al., 2018). The average mixing ratios of monoterpenes ($2.5 \pm 5.3$ ppb) in this study was also higher than that reported in a Norway spruce-dominated forest ($0.50 \pm 0.21$ ppb) in central Germany (Bourtsoukidis et al., 2014), but lower than that observed in the French Landes forest (~6 ppb) (Li et al., 2020). Relatively low mixing ratios of monoterpenes were reported previously for the boreal forests in Finland (~0.8 ppb) during summertime (Li et al., 2020; Mermet et al., 2021). Note that monoterpenes had a significant concentration variation in this study, which is attributed to the occurrence of monoterpene spikes (**Fig. 3d**). These monoterpene spikes were mainly related to the impact of BPP-related emissions as discussed in section 3.2. In this study, the average mixing ratios of sesquiterpenes measured by the CHARON-PTR-ToF-MS was $0.01 \pm 0.01$ ppb, a factor of two higher than that measured by the Vocus-PTR-ToF-MS. The average mixing ratios of sesquiterpenes was lower than that measured by a Vocus-PTR-ToF-MS in the French Landes forest (~0.06 ppb) (Li et al., 2020). It should be noted that the quantification of sesquiterpenes is affected by the degree of sesquiterpene fragmentation inside the PTR-ToF-MS, which can vary significantly depending on the instrument setting (Kim et al., 2009; Kari et al., 2018). In addition, sesquiterpenes may experience wall losses inside the inlet tubing and the instrument, and have low transmissions (Li et al., 2020). Due to a lack of a dedicated sesquiterpene calibration in this study, the quantification of sesquiterpenes measured by the PTR-ToF-MS can be regarded as the lower limit without the consideration of fragmentation.

### 3.1.3 Chemical composition of aerosol particles

During the entire campaign, the average mass concentrations of $PM_{2.5}$ and BC were $5.5 \pm 4.7$ µg m$^{-3}$ and $0.2 \pm 0.1$ µg m$^{-3}$ respectively (**Fig. S8**). The aerosol particle composition including organic aerosol (OA), nitrate, and ammonium measured by the CHARON-PTR-ToF-MS and BC by the aethalometer are simultaneously available from 22$^{nd}$-30$^{th}$ of June (**Fig. 4**). During this period, the average mass concentrations of OA was $0.8 \pm 0.5$ µg m$^{-3}$, accounting for $15 \pm 6$ % of $PM_{2.5}$ mass. The mass fraction of CHARON-PTR-ToF-MS-measured OA in $PM_{2.5}$ was close to that of semi-volatile oxygenated organic aerosol in $PM_{2.5}$ (9%-13%) resolved from the PMF analysis of OA measured by an aerosol mass spectrometer (AMS) in urban and rural environments (Song et al., 2022; Huang et al., 2019). The elemental ratios of OA (O:C and H:C) measured by the CHARON-PTR-ToF-MS were $0.32 \pm 0.03$ and $1.56 \pm 0.10$, respectively, which are comparable to the values of semi-volatile oxygenated organic aerosol (O:C: $0.35 \pm 0.14$ and H:C: $1.55 \pm 0.10$) resolved from the AMS-PMF analysis in previous studies (Ng et al., 2011; Ng et al., 2010). These results indicate that the OA mass detected by the CHARON-PTR-ToF-MS is mainly composed of semi-volatile organic compounds in this study. Please note that the fragmentation of organic compounds in the CHARON-PTR-ToF-MS may result in low average O:C values of bulk OA compared to those measured by the AMS (Leglise et al., 2019).

Mass concentrations of OA associated with individual *m/z* signals detected by the CHARON-PTR-ToF-MS ranged from ~0.1 to ~65 ng m$^{-3}$. In total, 164 organic ions can be well assigned with the chemical formula of $C_xH_y^+$ or $C_xH_yO_z^+$, contributing to $67 \pm 11$ % of total OA mass measured by the CHARON-PTR-ToF-MS. Furthermore, the organic ions assigned were mainly distributed in the $C_2$-$C_{10}$ range with oxygen atom numbers of 0-5 (**Fig. 4d**). Müller et al., (2017) observed a similar mass distribution of OA measured by the CHARON-PTR-ToF-MS in Valencia, Spain which was associated with the oxidation of abundant monoterpenes emitted from trees. With the same instrument, Gkatzelis et al., (2018) also reported a similar chemical composition of OA from the oxidation of tree emissions dominated by α-pinene and β-pinene in simulation chamber experiments. The abundant species in the $C_2$-$C_8$ range (**Fig. 4d**) are most likely fragments from $C_{9-10}$-monoterpene derived oxidized products which are prone to fragmentation in the CHARON-PTR-ToF-MS (Gkatzelis et al., 2018). Leglise et al., (2019) and Peng et al., (2023) further confirm the fragmentation of oxygenated organic compounds inside the CHARON-PTR-ToF-MS via the loss of neutral water, carbonyl, or carboxyl groups (-$H_2O$, -CO and -$CO_2$). For instance, *cis*-pinonic acid ($C_{10}H_{17}O_3^+$) a monoterpene oxidation

product as detected by the CHARON-PTR-ToF-MS can produce the typical fragment ions of $C_4H_7O^+$, $C_6H_{11}O_2+$ and $C_{10}H_{15}O_2^+$ (Peng et al., 2023; Leglise et al., 2019). Furthermore, the relative abundance of fragment ions ($C_4H_7O^+$, $C_6H_{11}O_2+$ and $C_{10}H_{15}O_2^+$) were generally higher than the parent ion $C_{10}H_{17}O_3^+$ (Leglise et al., 2019; Peng et al., 2023). In this study, we found that only a small fraction of the *cis*-pinonic acid parent ion $C_{10}H_{17}O_3^+$ was detected by the CHARON-PTR-ToF-MS compared to the fragment ions $C_4H_7O^+$, $C_6H_{11}O_2^+$ and $C_{10}H_{15}O_2^+$. Similarly, other monoterpene oxidation products such as $C_9H_{15}O_3^+$ (e.g., norpinonic acid) and $C_8H_{13}O_4^+$ (e.g., norpinic acid) showed lower abundances at their parent ions compared to their fragment ions with one $H_2O$ molecule lost ($C_9H_{13}O_2^+$ and $C_8H_{11}O_3^+$) (**Fig. S9**). We observed good correlations between $C_9H_{15}O_3^+$ and $C_9H_{13}O_2^+$ (r = 0.73), as well as between $C_8H_{13}O_4^+$ and $C_8H_{11}O_3^+$ (r =0.97), indicating that $C_9H_{13}O_2^+$ and $C_8H_{11}O_3^+$ are fragment ions from parent compounds. Previous studies have shown that the fragmentation pattern of oxidized organic compounds in the CHARON-PTR-ToF-MS varied depending on the instrument settings (Leglise et al., 2019; Gkatzelis et al., 2018). Therefore, we cannot compare the fragmentation patterns of organic compounds from our instruments with those from other studies. However, it is consistent with other studies that the particulate oxidized organic compounds measured by the CHARON-PTR-ToF-MS in this study were mainly detected as the more abundant fragment ions after losing one $H_2O$ molecule rather than as the parent ions.

**3.2 Meteorological impacts on the variations of BVOCs**

We firstly analyzed the variations in the mixing ratios of gas species as a function of wind direction (WD) with a bin of 10° (**Fig. 5**). According to the wind and geographical conditions around the sampling site (**Fig. 1b**), we divided the entire measurement period into four WD sectors including WD-forest (0-120°)), WD-cut (120-240°), WD-BPP (240-300°) and WD-village (300-330°). Within the sectors of WD-forest and WD-cut, the sampling site was influenced by an intact forest dominated by Norway spruce and a clear-cut area, respectively. In contrast, the sampling site was influenced by the winds coming from the BPP and the village residential areas within the sectors of WD-BPP and WD-village, respectively. We observed that the mixing ratios of $CH_4$ increased significantly in the WD-BPP along with the decrease of wind speeds and PBL heights and corresponding weaker dilution. In contrast, constantly low mixing ratios of $CH_4$ were observed in the WD-forest and WD-cut even when both wind speeds and PBL decreased significantly. The results indicate that the enhancement in $CH_4$ mixing ratios in the WD-BPP was mainly attributed to the BPP emissions. In addition, $CH_4$ mixing ratios remained higher for WD-village, which was likely associated with the anthropogenic emissions

407    from the village residential areas. We also observed a significant increase of monoterpene

408    mixing ratios in the WD-BPP along with lower ambient temperature (~15 °C) and decreasing

409    radiation. This suggests that the increase of monoterpene mixing ratios in the WD-BPP was due

410    to BPP emissions rather than biogenic emissions. In contrast to $CH_4$, monoterpenes showed

411    very low values in the WD-village, suggesting a minor contribution of anthropogenic emissions

412    from the village residential areas to monoterpenes.

413        We also observed significant variations in the mixing ratios of isoprene, monoterpene and

414    sesquiterpene in the WD-forest and WD-cut, likely associated with changes in meteorological

415    conditions, biogenic emissions and/or chemical oxidation processes. Specifically, the mixing

416    ratios of monoterpenes and sesquiterpenes increased in the WD-forest of 0-30° but isoprene

417    showed no significant change. The meteorological condition in the WD-forest of 0-30° was

418    characterized by low ambient temperature, low wind speed and shallow PBL during nighttime.

419    Unlike isoprene, monoterpenes and sesquiterpenes can still be released from the Norway spruce

420    in the dark (Van Meeningen et al., 2017). Monoterpenes and sesquiterpenes could accumulate

421    during nighttime in the WD-forest of 0-30° as a result of low concentrations of atmospheric

422    oxidants like $O_3$. Besides, we observed an increase of isoprene mixing ratios in the WD-forest

423    of 60-120° which was coincided with the increases of wind speed, PBL, ambient temperature

424    and radiation during daytime. In contrast, monoterpenes and sesquiterpenes showed low mixing

425    ratios of in the WD-forest of 60-120°. It is expected that higher temperature and radiation

426    enhanced biogenic emissions, resulting in the increase of isoprene mixing ratios. However,

427    lower mixing ratios of monoterpenes and sesquiterpenes were likely attributed to the

428    photochemical oxidation exceeding their biogenic emissions. The strong photochemical

429    oxidation processes were characterized by higher radiation and $O_3$ mixing ratios in the WD-

430    forest of 60-120°. In the WD-cut of 120-180°, we observed simultaneous increase of isoprene,

431    monoterpenes and sesquiterpenes, which were associated with enhanced biogenic emissions

432    induced by higher temperature. Conversely, simultaneous decrease of isoprene, monoterpenes

433    and sesquiterpenes mixing ratios were observed in the WD-cut of 180-240° along with high

434    ambient temperature. Note that the sampling site were more influenced by the distant Norway

435    Spruce trees in the WD-cut of 120-180° compared to the WD-cut of 180-240° (**Fig. 1a**). In

436    addition, the wind speeds were significantly higher in the WD-cut of 180-240°. Therefore, the

437    decreases in isoprene, monoterpenes and sesquiterpenes mixing ratios in the WD-cut of 180-

438    240° were attributed to the reduced biogenic emissions of fewer Norway spruce and the dilution

439    effect caused by higher wind speeds. The dilution effect was supported by the lowest CO mixing

440    ratios and BC mass concentrations observed in the WD-cut of 180-240°.

441    Based on the above WD analyses, we further investigated the diurnal variations of
442    meteorological parameters as well as gas species in two major groups influenced by
443    anthropogenic (WD-BPP and WD-village) and biogenic (WD-forest and WD-cut) emissions
444    respectively (**Fig. 6**). In the anthropogenic-group, the diurnal variations of $CH_4$ mixing ratios
445    showed higher values during nighttime, which were related to the BPP emissions, low wind
446    speed and PBL height. However, a less pronounced diurnal variations of $CH_4$ mixing ratios
447    were observed under the influence of biogenic-group. In the anthropogenic-group, the diurnal
448    behavior of monoterpenes showed higher mixing ratios during nighttime but with large
449    fluctuations over the whole day. These fluctuations with monoterpene spikes were related to
450    the BPP emissions depending on the wind directions. As expected, isoprene showed higher
451    concentrations during daytime in the biogenic-group, which is similar to the diurnal behavior
452    of isoprene emission rate in previous observations in Norway-spruce-dominated forests
453    (Bourtsoukidis et al., 2014; Juráň et al., 2017). However, in the biogenic-group, the diurnal
454    variations of monoterpenes and sesquiterpenes showed very low mixing ratios during daytime
455    due to the expanding PBL and strong photochemical consumption. The concentrations of
456    monoterpenes and sesquiterpenes peaked at ~18:00 when the concentrations of atmospheric
457    oxidants (OH radicals and $O_3$) and PBL heights decreased. Monoterpenes and sesquiterpenes
458    showed low mixing ratios with <1 ppb and <0.01 ppb, respectively after 18:00 during nighttime
459    in the biogenic-group. This is different with previous studies in the boreal forests where
460    constantly higher mixing ratios of monoterpenes and sesquiterpenes but lower $O_3$ values (<20
461    ppb) were observed during nighttime compared to daytime (Hakola et al., 2012; Li et al., 2020).
462    However, in our study, higher $O_3$ mixing ratios (~30 ppb) were observed during nighttime in
463    the biogenic-group, which may have reduced the concentrations of monoterpenes and
464    sesquiterpenes by nighttime oxidation. Note that the mixing ratios of monoterpenes and
465    sesquiterpenes were low during daytime, but they increased slightly from 8:00-12:00 when the
466    temperature and radiation increased. **Figure 7** shows the time series of isoprene, monoterpenes,
467    sesquiterpenes and $O_3$ along with wind direction and ambient temperature during low-T and
468    high-T episodes. During daytime of the high-T episode, we observed that the mixing ratios of
469    isoprene, monoterpenes, sesquiterpenes all increased as the temperature increased when the
470    sampling site was constantly influenced by the WD of ~100° from the intact forest. Meanwhile,
471    higher radiation and constantly high mixing ratios of $O_3$ (40-60 ppb) were observed during
472    daytime of the high-T episode. The photochemical $O_3$ production is supported by also by higher
473    BVOC mixing ratios. However, the increasing biogenic emissions due to higher temperatures
474    and solar radiation obviously exceeded the photochemical consumptions. Similarly, higher

475  mixing ratios of $O_3$ were observed during daytime of the low-T episode when the sampling site

476  was also constantly influenced by the wind direction of ~100° (e.g., 11th of June). However, the

477  mixing ratios of isoprene, monoterpenes, sesquiterpenes showed no increase. In **Fig. 7a**, we

478  also found that very high mixing ratios of monoterpenes and sesquiterpenes during the low-T

479  episode (e.g., 20:00-24:00, 10th of June) were associated with the changes of wind directions,

480  which was in line with the WD analyses as discussed above. Besides, soil moisture showed no

481  significant difference between the low-T and high-T episode (**Fig. 2**). We cannot demonstrate

482  the impact of soil moisture on the variations of BVOC mixing ratios due to the observation

483  period was short in this study.

484  **3.3 Source apportionment of VOCs**

485      In addition to meteorological impacts, the variations of VOC concentrations are influenced

486  by different emission sources and chemical processes. We performed a PMF analysis of Vocus-

487  PTR-ToF-MS-measured VOC data to identify and determine the impacts of different sources

488  and oxidation processes. According to the factor profiles and temporal variations, we present a

489  six-factor solution including one terpene-dominated factor, one factor related to BVOC

490  oxidation during nighttime, one factor related to aromatic VOC oxidation and three factors

491  related to daytime BVOC oxidation. **Figure 8** shows the factor profiles, time series and diurnal

492  variations of six factors as well as their relative contribution to total VOCs (TVOCs) during the

493  entire measurement campaign.

494      The first factor profile was dominated by the monoterpene parent ion ($C_{10}H_{17}^+$) and its

495  fragment ion ($C_6H_9^+$) (Tani et al., 2003; Kari et al., 2018). Furthermore, this factor was

496  characterized with higher fraction of monoterpenoids such as $C_{10}H_{17}O^+$ (camphor or

497  monoterpene oxide) and $C_{10}H_{19}O^+$ (linalool or monoterpene water cluster) in high mass range

498  ($m/z$ 140-230) (Li et al., 2020). These monoterpenoids can be emitted by leaves and flowers

499  directly (Joó et al., 2010). Therefore, we define this factor as a terpene-dominated factor. As

500  discussed before, the variations of monoterpene concentrations were influenced by the BPP

501  emissions and biogenic emissions depending on the wind directions. In this study, PMF analysis

502  could not separate the relative contribution of biogenic emissions and BPP emissions to

503  monoterpenes directly. This is probably due to the source profile of BPP emissions dominated

504  by the monoterpenes that is similar to that of biogenic emissions. Based on the WD analyses,

505  this factor was expected to be mainly associated with the biogenic emissions when the winds

506  were coming from the forest. In contrast, when the winds were coming from the BPP, this factor

507  was significantly contributed by the BPP emissions.

508    The second factor profile was characterized with high fractions of $C_{10}H_{17}O^+$ (monoterpene

509    oxide), $C_{10}H_{17}O_2^+$ and $C_{10}H_{15}O^+$ (pinonaldehyde and its fragment ion) in high mass range.

510    These compounds were weakly-oxidized products of monoterpenes with oxygen atom number

511    < 3 as found by previous studies (Li et al., 2021a; Li et al., 2020; Vermeuel et al., 2023). In

512    addition, this factor was dominated by $C_3H_7O^+$ (acetone), which could be contributed by the

513    primary emissions and the oxidation of VOCs from both biogenic and anthropogenic sources

514    (Jacob et al., 2002). The diurnal pattern of second factor showed higher concentrations at

515    nighttime. Therefore, we define this factor representing the secondary oxidation processes of

516    BVOCs especially monoterpenes during nighttime (night-SecVOC). Li et al., (2021a)

517    performed a binPMF analysis on Vocus-PTR-ToF-MS-measured VOC data at two European

518    forest sites. They also resolved a factor representing weakly-oxidized products of monoterpenes

519    with higher concentrations at night (Li et al., 2021a).

520    The third factor profile was characterized with higher fractions of $C_6H_7O^+$ (phenol),

521    $C_6H_7O_2^+$ (catechol), and $C_7H_7O_2^+$ (benzoic acid) compared to other factors. Furthermore, this

522    factor was dominated by $C_7H_9O_3^+$ (e.g., oxo-heptedienoic acid) and $C_8H_9O_3^+$ (e.g., vanillin) in

523    high mass range. These OVOC species could originate from the oxidation of aromatic

524    hydrocarbons (Hamilton et al., 2005; Zaytsev et al., 2019; Li et al., 2021b; Wu et al., 2014;

525    Lannuque et al., 2023). As expected, good correlations were found for aromatic OVOC with

526    catechol (r = 0.87 for $C_6H_7O_2^+$) and benzoic acid (r = 0.84 for $C_7H_7O_2^+$). In addition, this factor

527    also correlated well (r = 0.77-0.87, **Fig. S10**) with $C_5H_5O_3^+$ (e.g., methylfurandione), $C_5H_5O_2^+$

528    (e.g., butenedial), $C_4H_5O_2^+$ (e.g., furfural), and $C_3H_5O_2^+$ (e.g., methylglyoxal). These

529    compounds are likely ring-opening products of toluene oxidation as reported in previous studies

530    (Zaytsev et al., 2019; Wu et al., 2014; Lannuque et al., 2023). Therefore, we identified this

531    factor as a factor of aromatic OVOC representing the OVOCs formed from the oxidation of

532    aromatic hydrocarbons. The diurnal variation of aromatic OVOC factor showed slightly higher

533    concentrations during daytime, which can be related to an enhanced photochemical oxidation

534    of aromatic hydrocarbons.

535    In this study, we also resolved three factors related to the oxidation of BVOCs during

536    daytime denoted as day-SecVOC1, day-SecVOC2 and day-SecVOC3. The factor profile of

537    day-SecVOC1 was characterized with high fractions of acetic acid ($C_2H_5O_2^+$) as well as

538    isoprene and its oxidation products (e.g., $C_5H_9^+$, $C_4H_7O_{1-4}^+$ and $C_5H_9O_{2-4}^+$). This factor was also

539    dominated by stronger oxidized products of monoterpenes with oxygen atom numbers >3 (e.g.,

540    $C_{10}H_{17}O_{4-5}^+$) compared to other factors in the higher mass range. The diurnal variations of day-

541  SecVOC1 factor showed high concentrations during daytime. Therefore, the day-SecVOC1

542  factor can be mainly attributed to the photochemical oxidation of isoprene and monoterpenes

543  during daytime. Li et al., (2021a) resolved one factor representing isoprene and its oxidation

544  products and another factor representing stronger oxidized products of monoterpenes from the

545  binPMF analysis for a low-mass ($mz$50-200) and a high-mass range ($mz$201-320), respectively,

546  for two European forest sites. They found that these two factors had a similar diurnal pattern

547  with high daytime concentrations. In our study, we performed the PMF analysis for the full

548  mass range (m/z40-220) of the major VOC ions and resolved the day-SecVOC1 factor

549  containing high fractions of oxidized products of isoprene and monoterpenes. This suggests that

550  isoprene oxidation products and higher oxidized products of monoterpenes were mainly related

551  to the daytime oxidation processes. The factor profiles of both day-SecVOC2 and day-

552  SecVOC3 were characterized with high fractions of acetone ($C_3H_7O^+$) and acetic acid

553  ($C_2H_5O_2^+$). Acetone and acetic acid could be contributed by biogenic and anthropogenic

554  secondary sources (Khare et al., 1999; Jacob et al., 2002). The factor profile of day-SecVOC2

555  also had high fractions of $C_2H_7O_3^+$ (acetic acid water cluster), $C_3H_7O_2^+$ (propionic acid),

556  $C_4H_9O_2^+$ (butyric acid) and $C_3H_9O_2^+$ (e.g., propylene glycol). These gaseous organic acids could

557  be formed from the oxidation of BVOCs like monoterpenes (Friedman and Farmer, 2018). In

558  addition, the factor profile of day-SecVOC3 showed higher fractions of $C_4H_7O_4^+$ (e.g., succinic

559  acid) compared to other factors. The time series of day-SecVOC3 showed the highest

560  correlations with $C_2H_7O_3^+$ (acetic acid water cluster, r = 0.79), $C_2H_5O_2^+$ (acetic acid, r = 0.63)

561  and $C_3H_9O_3^+$ (propionic acid water cluster) compared to other factors. The time series of day-

562  SecVOC3 factor also showed strong correlations with $C_4H_6O^+$ (r = 0.90, **Fig. S10**) and $C_2H_5O_3^+$

563  (r = 0.89), which can be assigned as the isoprene oxidation product as deprotonated $C_4H_7O^+$

564  (MVK+MACR) and glycolic acid, respectively. In addition, $O_3$ was only weakly correlated

565  with day-SecVOC2 (r = 0.27), but much better correlated with day-SecVOC3 (r = 0.57).

566  Moreover, a better correlation was found between $O_3$ and the sum of these two factors (r =

567  0.70). The diurnal variations of both factors showed higher concentrations during daytime.

568  Based on these results, we identified day-SecVOC2 and day-SecVOC3 as representing low-

569  molecular weight oxygenated organic compounds produced from the daytime photooxidation

570  of BVOCs.

571      As shown in **Fig. 8**, the mixing ratios of TVOCs measured by the Vocus-PTR-ToF-MS for

572  the PMF analysis was 9.0 ± 4.4 ppb during the entire campaign. The mixing ratios of TVOCs

573  was dominated by the daytime BVOC oxidation with day-SecVOC1 (8% ± 5%), day-SecVOC2

574  (27% ± 20%), day-SecVOC3 (18% ± 21%). This indicates substantial contributions of

575    oxygenated species to TVOCs during the entire campaign. Based on the WD analysis, we

576    further compared the relative contributions of VOC factors to TVOCs for the groups influenced

577    by the biogenic and anthropogenic emissions, respectively. The average concentration of

578    TVOCs in the biogenic-group (9.7 ± 4.7 ppb) were slightly higher than that in the

579    anthropogenic-group (7.1 ± 3.6 ppb). The contribution of day-SecVOC2 to TVOCs was

580    comparable with 25% ± 21% and 32% ± 18% for the biogenic- and anthropogenic-group,

581    respectively. However, the contribution of day-SecVOC3 to TVOCs in the biogenic-group

582    (26% ± 25%) was higher than that in the anthropogenic-group (13% ± 15%). We observed

583    significantly elevated mixing ratios of isoprene (**Fig. 3c**) and day-SecVOC3 during the high-T

584    episode (**Fig. 8**). As mentioned before, the sampling site was mainly influenced by the winds

585    coming from the forest during high-T episode along with higher mixing ratios of $O_3$. Therefore,

586    higher contribution of day-SecVOC3 in the biogenic-group was attributed to the strong

587    oxidation of BVOCs especially of isoprene. The contribution of terpene-dominated factor to

588    TVOCs was higher in the anthropogenic-group (18% ± 16%) compared to that in the biogenic-

589    group (11% ± 15%). This is consistent with the WD analyses that higher monoterpene mixing

590    ratios were related to the BPP emissions. In addition, the contributions of night-SecVOC and

591    day-SecVOC1 factors to TVOCs concentrations were slightly higher in the anthropogenic-

592    group, which were related to high abundances of monoterpenes. Furthermore, gas-to-particle

593    partitioning processes could also influence the variations of BVOC oxidation products and thus

594    night-SecVOC and day-SecVOC1 factors.

595    **3.4 Variations of BVOC oxidation products in gas- and particle phases**

596    **Figure 9** shows the diurnal variations of concentrations of organic molecules ($C_5H_9O_{1-4}^+$,

597    $C_4H_7O_{1-4}^+$, $C_{10}H_{17}O_{1-5}^+$ and $C_{10}H_{15}O_{1-5}^+$) in the gas phase measured by the Vocus-PTR-ToF-

598    MS and particle phase compounds measured by the CHARON-PTR-ToF-MS during $22^{nd}$-$30^{th}$

599    of June. These organic molecules are important components of night-SecVOC and day-

600    SecVOC1 factors resolved by the PMF analysis, and they are identified as the oxidation

601    products from isoprene and monoterpenes based on previous field observations and simulation

602    chamber experiments (Gkatzelis et al., 2018; Li et al., 2020). For example, gaseous $C_4H_7O^+$ can

603    be the sum of methyl vinyl ketone (MVK) and methacrolein (MACR), which are major products

604    of the isoprene oxidation (Wennberg et al., 2018). $C_{10}H_{17}O_3^+$ can be attributed to *cis*-pinonic

605    acid formed from the oxidation of monoterpenes (e.g., α-pinene). Again, the fragmentation of

606    high-molecular weight oxidized organic compounds measured by the PTR-ToF-MS

607    instruments could produce the fragment ions via the loss of neutral water, carbonyl, or carboxyl

608    groups ($-H_2O$, $-CO$ and $-CO_2$). The diurnal variations of all isoprene oxidation products

609    ($C_5H_9O_{1-4}^+$ and $C_4H_7O_{1-4}^+$) in both gas and particle phases showed higher concentrations from

610    morning (6:00-8:00) to afternoon (12:00-16:00) as well as isoprene itself. These results indicate

611    that higher temperatures and intensive sunlight not only favor the isoprene emissions but also

612    enhance photochemical oxidation of isoprene. Besides, we found that the concentrations of

613    particulate $C_4H_7O_{1-2}^+$ showed increased values from early nighttime (18:00-20:00) to midnight

614    (0:00-2:00 of the next day). As mentioned before, the fragmentation of *cis*-pinonic acid in the

615    CHARON-PTR-ToF-MS can produce the fragment ions $C_4H_7O^+$, $C_6H_{11}O_2+$ and $C_{10}H_{15}O_2^+$

616    (Gkatzelis et al., 2018; Peng et al., 2023; Muller et al., 2017; Leglise et al., 2019). Furthermore,

617    we observed a similar diurnal pattern of $C_4H_7O^+$ and $C_{10}H_{15}O_2^+$ in the particle phase, suggesting

618    that the nighttime increase of particulate $C_4H_7O^+$ was likely contributed by the fragmentation

619    of *cis*-pinonic acid. Due to instrumental limitation, it is difficult to assign each ion detected by

620    the PTR-ToF-MS to either parent ion or fragment ion of one organic compound in the ambient

621    particles.

622         The diurnal variations of weakly-oxidized products of monoterpenes like $C_{10}H_{17}O_{1-2}^+$ and

623    $C_{10}H_{15}O_{1-2}^+$ in both gas and particle phases showed elevated concentrations during nighttime.

624    In contrast, the more-oxidized products of monoterpenes ($C_{10}H_{17}O_{4-5}^+$ and $C_{10}H_{15}O_{4-5}^+$) showed

625    higher concentrations in gas and particle phases during daytime. The higher atmospheric

626    oxidation capacity during daytime compared to nighttime leads to the formation of more-

627    oxidized products. In addition, $C_{10}H_{17}O_3^+$ (*cis*-pinonic acid) and its fragment ion ($C_{10}H_{15}O_2^+$)

628    in the gas phase showed less pronounced diurnal patterns. The particulate $C_{10}H_{17}O_3^+$ also

629    showed a less pronounced diurnal behavior, while the particulate $C_{10}H_{15}O_2^+$ showed increased

630    concentrations during nighttime. This is in agreement with previous findings that most of the

631    particulate compounds detected by the CHARON-PTR-ToF-MS were not detected as the parent

632    ion but as the fragment ion with one $H_2O$ molecule lost (Gkatzelis et al., 2018). In this study,

633    $C_{14}H_{23}O_2^+$, $C_{15}H_{23}O^+$, $C_{15}H_{25}O_2^+$ were measured by the PTR instruments, which can be

634    considered as the sesquiterpene oxidation products based on previous field and simulation

635    chamber studies. Here $C_{14}H_{23}O_2^+$ was detected only in the gas phase by the Vocus-PTR-ToF-

636    MS, while $C_{15}H_{23}O_2^+$ and $C_{15}H_{25}O_2^+$ were detected only in the particle phase by the CHARON-

637    PTR-ToF-MS. The concentrations of sesquiterpene oxidation products in both gas (<0.5 ppt)

638    and particle phases (<5 ng m$^{-3}$) were relatively low probably due to correspondingly low

639    concentrations of sesquiterpenes in this study. The diurnal pattern of gaseous $C_{14}H_{23}O_2^+$ showed

640    two peaks in the morning and early evening (**Fig. S11**), which was similar to those of weakly-

641    oxidized products of sesquiterpenes (e.g., $C_{14}H_{22}O_{1-3}$ and $C_{15}H_{24}O_{1-3}$) observed at the Landes

642 forest in France (Li et al., 2020). The diurnal variations of particulate $C_{15}H_{23}O_2^+$ and $C_{15}H_{25}O_2^+$

643 showed slightly higher values during nighttime.

644     Furthermore, we calculated the variations of OA/ΔCO, which are the total OA

645 concentrations measured by the CHARON-PTR-ToF-MS normalized over ΔCO (subtracted by

646 the background CO concentration) during 22$^{nd}$-30$^{th}$ of June (**Fig. 10**). CO is relatively long-

647 lived, normalizing the observed OA mass concentrations to the background-corrected CO helps

648 to minimize the impacts of boundary layer dynamics (De Gouw and Jimenez, 2009). An

649 increase of OA/ΔCO was observed during nighttime of the high-T episode, which could be

650 related to the gas-to-particle partitioning of BVOC oxidation products. Based on the two PTR

651 measurements, we calculated the particulate fraction of representative monoterpene oxidation

652 products (i.e., $C_{10}H_{17}O_{1-3}^+$ and $C_{10}H_{15}O_{1-5}^+$) to estimate their gas gas-to-particle partitioning

653 processes. The two PTR instruments used in this study may have different sensitivities or

654 fragmentation for different oxygenated organic compounds. For example, the concentrations of

655 monoterpene oxidation products such as $C_9H_{15}O^+$, $C_{10}H_{15}O_{1-2}^+$ and $C_{10}H_{17}^+$ measured by the

656 Vocus-PTR-ToF-MS were ~2-3 times higher than those measured by the CHARON-PTR-ToF-

657 MS (**Fig. S13b**). Although we cannot precisely calculate the $F_p$ values for each OA molecule

658 due to instrumental limitations, the variations of calculated $F_p$ values can still be used as an

659 indicator for estimating the gas-to-particle portioning processes. As shown in **Fig. 10**, weakly-

660 oxidized molecules of monoterpenes ($C_{10}H_{17}O_{1-2}^+$ and $C_{10}H_{15}O_{1-3}^+$) had lower $F_p$ values

661 compared to more-oxidized molecules of monoterpenes ($C_{10}H_{17}O_3^+$ and $C_{10}H_{15}O_{4-5}^+$). This is

662 expected because more-oxidized products of monoterpenes generally have lower volatility

663 compared to weakly-oxidized ones. Interestingly, the $F_p$ values of weakly-oxidized molecules

664 of monoterpenes showed similar temporal trends as the relative humidity. Especially for the

665 high-T episode, the $F_p$ values of weakly-oxidized molecules of monoterpenes ($C_{10}H_{15}O_{1-3}^+$)

666 showed positive correlations (r = 0.65-0.71) with RH. This indicates that increasing RH can

667 enhance the particle fraction of weakly-oxidized molecules of monoterpenes and thus increase

668 SOA mass. As validated in Section 3.3, these weakly-oxidized molecules of monoterpenes are

669 formed by oxidation of monoterpenes emitted from trees during the high-T episode rather than

670 from BPP emissions. It is reasonable to assume that these monoterpenes are mainly α-pinene

671 and β-pinene because our sampling site was in a forest dominated by Norway spruce known to

672 emit mainly pinenes (Christensen et al., 2000; Hakola et al., 2017). Previously, Tillmann et al.,

673 (2010) found that the SOA yields from the ozonolysis of α-pinene were higher at humid

674 conditions than at dry conditions. More recently, Surdu et al., (2023) studied the effect of RH

675 on the partitioning of oxidized organic molecules formed from α-pinene oxidation at the CERN

676 CLOUD chamber. They observed that the particle-phase concentrations of semi-volatile

677 organic molecules ($C_{10}H_{16}O_{2-3}$) from α-pinene oxidation significantly increases by factors of 2-

678 4 with increasing RH, thus leading to a substantial increase of SOA mass (Surdu et al., 2023).

679 Similarly, Luo et al., (2024) reported that increasing RH from 3% to 84% increase the

680 abundance of less oxidized products (e.g., $C_{10}H_{16}O_{2-6}$) from α-pinene ozonolysis. In our study,

681 during the high-T episode, we observed the $F_p$ values for $C_{10}H_{15}O^+$, $C_{10}H_{15}O_2^+$ and $C_{10}H_{15}O_3^+$

682 increased by ~2%, ~6% and ~20% respectively when RH was increased from 30-40% to 60-

683 80%. Besides, the ambient temperature was anticorrelated with RH in this study. Thus, lower

684 temperatures may further additionally favor the gas-to-particle partitioning of semi-volatile

685 organic molecules from monoterpene oxidation.

686 **4 Conclusions**

687 In this study, we investigated the characteristics of VOCs and OA particles simultaneously

688 measured by a CHARON-PTR-ToF-MS and a Vocus-PTR-ToF-MS at a Norway-spruce-

689 dominated forest stressed by bark beetles and droughts close to a BPP in western Germany

690 during June 2020. The average mass concentration of OA particles detected by the CHARON-

691 PTR-ToF-MS was $0.8 \pm 0.5$ µg m$^{-3}$. The chemical composition of OA ions ranged between $C_2$

692 and $C_{10}$ with oxygen atom numbers of 0-5, which were mainly attributed to the semi-volatile

693 organic compounds formed from monoterpene oxidation. The average mixing ratios of isoprene

694 and monoterpenes were higher than the values previously measured in both German temperate

695 forests and boreal forests during summertime (Mermet et al., 2021; Li et al., 2021a; Hellén et

696 al., 2018; Bourtsoukidis et al., 2014) which may be due to stressed trees with long lasting

697 droughts and bark beetle infestation and differences in the meteorological conditions. Based on

698 the WD analyses, BVOC data were categorized into two groups to distinguish the impacts of

699 biogenic emissions from an intact forest and a clear cut (biogenic-group) and anthropogenic

700 emissions from a BPP and a village (anthropogenic-group). The mixing ratios of $CH_4$ and

701 monoterpenes showed significantly higher values in the anthropogenic-group. This was

702 expected for $CH_4$, and it is also known that BPP can release high concentrations of

703 monoterpenes during biowaste storage and fermentation processes (Salazar Gómez et al., 2016;

704 Papurello et al., 2012). In the biogenic-group, the variations in mixing ratios of isoprene,

705 monoterpenes and sesquiterpenes were driven by the interplay between meteorological

706 conditions, biogenic emissions and subsequent chemical oxidation processes. Based on the

707 PMF analysis of VOCs measured by the Vocus-PTR-ToF-MS, six factors were resolved,

708 representing the major sources and/or products of chemical transformation processes. During

the entire measurement period, TVOCs were largely composed of oxygenated organic compounds formed from the photochemical oxidation of BVOCs during daytime. However, monoterpenes and their weakly-oxidized products (e.g., $C_{10}H_{15}O_{1-3}^+$ and $C_{10}H_{17}O_{1-2}^+$) dominated the TVOCs during nighttime. These weakly-oxidized monoterpene products in the particle phase also showed higher mixing ratios during nighttime. In contrast, more-oxidized monoterpene products (e.g., $C_{10}H_{17}O_{4-5}^+$ and $C_{10}H_{15}O_{4-5}^+$) in both gas and particle phases were more abundant during daytime. By combining the gas and particle data measured by the CHARON-PTR-ToF-MS and the Vocus-PTR-ToF-MS, we found that increasing RH and decreasing temperature led to an increase in the particulate fraction of weakly-oxidized monoterpene products, consistent with the findings from recent simulation chamber studies (Surdu et al., 2023; Luo et al., 2024). Overall, this study demonstrates that the variations of BVOCs are influenced not only by meteorology and biogenic emissions but also by local anthropogenic emissions (e.g., from a BPP), and subsequent chemical transformation processes in a typical stressed European coniferous forest. The impact of soil moisture, tree species composition and tree health conditions on the variations of BVOC concentrations could not be fully addressed due to the relative short observation period. Future long-term field measurements including seasonality and detailed tree characterization are necessary to assess the impacts of droughts and bark beetle outbreaks on BVOC emissions and subsequent formation of SOA.

**Data availability**

Data shown in the paper are available via the KIT data repository KITopen (link will be added).

**Author contributions**

JS, HS and RT conducted the field measurements. JS and GG carried out the data analysis of CHARON-PTR-ToF-MS and Vocus-PTR-ToF-MS respectively. NB and TL gave general comments for this paper. JS drafted the manuscript with contributions from all co-authors.

**Competing interest**

At least one of the (co-)authors is a member of the editorial board of Atmospheric Chemistry and Physics.

**Acknowledgement**

This work was supported by the Modular Observation Solutions for Earth Systems (MOSES) project, a novel observing system of the Helmholtz Association. Financial support by China

741 Scholarship Council (CSC) for JS is gratefully acknowledged. We gratefully acknowledged the

742 TERENO (Terrestrial Environmental Observatories) funded by the Helmholtz-Gemeinschaft.

743 The authors acknowledged Heye Bogena for providing daily soil moisture data as well as

744 Christian Wesolek, Sergej Wedel, and Doreen Niether for their technical support in field

745 measurement deployment.

746

## References

Atkinson, R.: Atmospheric chemistry of VOCs and NOx, Atmos. Environ., 34, 2063-2101, https://doi.org/10.1016/S1352-2310(99)00460-4, 2000.

Bakkaloglu, S., Lowry, D., Fisher, R. E., France, J. L., Brunner, D., Chen, H., and Nisbet, E. G.: Quantification of methane emissions from UK biogas plants, Waste Manage, 124, 82-93, https://doi.org/10.1016/j.wasman.2021.01.011, 2021.

Bogena, H. R., Huisman, J. A., Güntner, A., Hübner, C., Kusche, J., Jonard, F., Vey, S., and Vereecken, H.: Emerging methods for noninvasive sensing of soil moisture dynamics from field to catchment scale: a review, WIREs Water, 2, 635-647, https://doi.org/10.1002/wat2.1097, 2015.

Bonn, B., Magh, R. K., Rombach, J., and Kreuzwieser, J.: Biogenic isoprenoid emissions under drought stress: different responses for isoprene and terpenes, Biogeosciences, 16, 4627-4645, 10.5194/bg-16-4627-2019, 2019.

Bourtsoukidis, E., Williams, J., Kesselmeier, J., Jacobi, S., and Bonn, B.: From emissions to ambient mixing ratios: online seasonal field measurements of volatile organic compounds over a Norway spruce-dominated forest in central Germany, Atmos. Chem. Phys., 14, 6495-6510, 10.5194/acp-14-6495-2014, 2014.

Bourtsoukidis, E., Pozzer, A., Williams, J., Makowski, D., Peñuelas, J., Matthaios, V. N., Lazoglou, G., Yañez-Serrano, A. M., Lelieveld, J., Ciais, P., Vrekoussis, M., Daskalakis, N., and Sciare, J.: High temperature sensitivity of monoterpene emissions from global vegetation, Communications Earth & Environment, 5, 23, 10.1038/s43247-023-01175-9, 2024.

Brémond, U., Bertrandias, A., Steyer, J.-P., Bernet, N., and Carrere, H.: A vision of European biogas sector development towards 2030: Trends and challenges, J. Clean. Prod., 287, 125065, https://doi.org/10.1016/j.jclepro.2020.125065, 2021.

Byron, J., Kreuzwieser, J., Purser, G., van Haren, J., Ladd, S. N., Meredith, L. K., Werner, C., and Williams, J.: Chiral monoterpenes reveal forest emission mechanisms and drought responses, Nature, 609, 307-312, 10.1038/s41586-022-05020-5, 2022.

Christensen, C. S., Hummelshøj, P., Jensen, N. O., Larsen, B., Lohse, C., Pilegaard, K., and Skov, H.: Determination of the terpene flux from orange species and Norway spruce by relaxed eddy accumulation, Atmos. Environ., 34, 3057-3067, https://doi.org/10.1016/S1352-2310(99)00502-6, 2000.

De Gouw, J. and Jimenez, J. L.: Organic Aerosols in the Earth's Atmosphere, Environ. Sci. Technol., 43, 7614-7618, 10.1021/es9006004, 2009.

Desservettaz, M., Pikridas, M., Stavroulas, I., Bougiatioti, A., Liakakou, E., Hatzianastassiou, N., Sciare, J., Mihalopoulos, N., and Bourtsoukidis, E.: Emission of volatile organic compounds from residential biomass burning and their rapid chemical transformations, Science of The Total Environment, 903, 166592, https://doi.org/10.1016/j.scitotenv.2023.166592, 2023.

Eichler, P., Muller, M., D'Anna, B., and Wisthaler, A.: A novel inlet system for online chemical analysis of semi-volatile submicron particulate matter, Atmos. Meas. Tech., 8, 1353-1360, 10.5194/amt-8-1353-2015, 2015.

Faiola, C. and Taipale, D.: Impact of insect herbivory on plant stress volatile emissions from trees: A synthesis of quantitative measurements and recommendations for future research, Atmospheric Environment: X, 5, 100060, https://doi.org/10.1016/j.aeaoa.2019.100060, 2020.

Friedman, B. and Farmer, D. K.: SOA and gas phase organic acid yields from the sequential photooxidation of seven monoterpenes, Atmos. Environ., 187, 335-345, https://doi.org/10.1016/j.atmosenv.2018.06.003, 2018.

Ghimire, R. P., Kivimäenpää, M., Blomqvist, M., Holopainen, T., Lyytikäinen-Saarenmaa, P., and Holopainen, J. K.: Effect of bark beetle (Ips typographus L.) attack on bark VOC emissions of Norway spruce (Picea abies Karst.) trees, Atmospheric Environment, 126, 145-152, https://doi.org/10.1016/j.atmosenv.2015.11.049, 2016.

Gkatzelis, G. I., Coggon, M. M., McDonald, B. C., Peischl, J., Gilman, J. B., Aikin, K. C., Robinson, M. A., Canonaco, F., Prevot, A. S. H., Trainer, M., and Warneke, C.: Observations Confirm that Volatile Chemical Products Are a Major Source of Petrochemical Emissions in U.S. Cities, Environ. Sci. Technol., 55, 4332-4343, 10.1021/acs.est.0c05471, 2021.

Gkatzelis, G. I., Tillmann, R., Hohaus, T., Müller, M., Eichler, P., Xu, K. M., Schlag, P., Schmitt, S. H., Wegener, R., Kaminski, M., Holzinger, R., Wisthaler, A., and Kiendler-Scharr, A.: Comparison of

802     three aerosol chemical characterization techniques utilizing PTR-ToF-MS: a study on freshly
803     formed and aged biogenic SOA, Atmos. Meas. Tech., 11, 1481-1500, 10.5194/amt-11-1481-2018,
804     2018.
805 Guenther, A. B., Jiang, X., Heald, C. L., Sakulyanontvittaya, T., Duhl, T., Emmons, L. K., and Wang,
806     X.: The Model of Emissions of Gases and Aerosols from Nature version 2.1 (MEGAN2.1): an
807     extended and updated framework for modeling biogenic emissions, Geosci. Model Dev., 5, 1471-
808     1492, 10.5194/gmd-5-1471-2012, 2012.
809 Hakola, H., Hellén, H., Hemmilä, M., Rinne, J., and Kulmala, M.: In situ measurements of volatile
810     organic compounds in a boreal forest, Atmos. Chem. Phys., 12, 11665-11678, 10.5194/acp-12-
811     11665-2012, 2012.
812 Hakola, H., Tarvainen, V., Praplan, A. P., Jaars, K., Hemmilä, M., Kulmala, M., Bäck, J., and Hellén,
813     H.: Terpenoid and carbonyl emissions from Norway spruce in Finland during the growing season,
814     Atmos. Chem. Phys., 17, 3357-3370, 10.5194/acp-17-3357-2017, 2017.
815 Hallquist, M., Wenger, J. C., Baltensperger, U., Rudich, Y., Simpson, D., Claeys, M., Dommen, J.,
816     Donahue, N. M., George, C., Goldstein, A. H., Hamilton, J. F., Herrmann, H., Hoffmann, T., Iinuma,
817     Y., Jang, M., Jenkin, M. E., Jimenez, J. L., Kiendler-Scharr, A., Maenhaut, W., McFiggans, G.,
818     Mentel, T. F., Monod, A., Prévôt, A. S. H., Seinfeld, J. H., Surratt, J. D., Szmigielski, R., and Wildt,
819     J.: The formation, properties and impact of secondary organic aerosol: current and emerging issues,
820     Atmos. Chem. Phys., 9, 5155-5236, 10.5194/acp-9-5155-2009, 2009.
821 Hamilton, J. F., Webb, P. J., Lewis, A. C., and Reviejo, M. M.: Quantifying small molecules in
822     secondary organic aerosol formed during the photo-oxidation of toluene with hydroxyl radicals,
823     Atmospheric Environment, 39, 7263-7275, https://doi.org/10.1016/j.atmosenv.2005.09.006, 2005.
824 Hellén, H., Praplan, A. P., Tykkä, T., Ylivinkka, I., Vakkari, V., Bäck, J., Petäjä, T., Kulmala, M., and
825     Hakola, H.: Long-term measurements of volatile organic compounds highlight the importance of
826     sesquiterpenes for the atmospheric chemistry of a boreal forest, Atmos. Chem. Phys., 18, 13839-
827     13863, 10.5194/acp-18-13839-2018, 2018.
828 Hersbach, H., Bell, B., Berrisford, P., Hirahara, S., Horányi, A., Muñoz-Sabater, J., Nicolas, J., Peubey,
829     C., Radu, R., Schepers, D., Simmons, A., Soci, C., Abdalla, S., Abellan, X., Balsamo, G., Bechtold,
830     P., Biavati, G., Bidlot, J., Bonavita, M., De Chiara, G., Dahlgren, P., Dee, D., Diamantakis, M.,
831     Dragani, R., Flemming, J., Forbes, R., Fuentes, M., Geer, A., Haimberger, L., Healy, S., Hogan, R.
832     J., Hólm, E., Janisková, M., Keeley, S., Laloyaux, P., Lopez, P., Lupu, C., Radnoti, G., de Rosnay,
833     P., Rozum, I., Vamborg, F., Villaume, S., and Thépaut, J.-N.: The ERA5 global reanalysis, Quarterly
834     Journal of the Royal Meteorological Society, 146, 1999-2049, https://doi.org/10.1002/qj.3803,
835     2020.
836 Huang, W., Saathoff, H., Shen, X., Ramisetty, R., Leisner, T., and Mohr, C.: Chemical Characterization
837     of Highly Functionalized Organonitrates Contributing to Night-Time Organic Aerosol Mass
838     Loadings and Particle Growth, Environ. Sci. Technol., 53, 1165-1174, 10.1021/acs.est.8b05826,
839     2019.
840 Huang, W., Li, H., Sarnela, N., Heikkinen, L., Tham, Y. J., Mikkilä, J., Thomas, S. J., Donahue, N. M.,
841     Kulmala, M., and Bianchi, F.: Measurement report: Molecular composition and volatility of gaseous
842     organic compounds in a boreal forest – from volatile organic compounds to highly oxygenated
843     organic molecules, Atmos. Chem. Phys., 21, 8961-8977, 10.5194/acp-21-8961-2021, 2021.
844 Isaacman-VanWertz, G., Yee, L. D., Kreisberg, N. M., Wernis, R., Moss, J. A., Hering, S. V., de Sá, S.
845     S., Martin, S. T., Alexander, M. L., Palm, B. B., Hu, W., Campuzano-Jost, P., Day, D. A., Jimenez,
846     J. L., Riva, M., Surratt, J. D., Viegas, J., Manzi, A., Edgerton, E., Baumann, K., Souza, R., Artaxo,
847     P., and Goldstein, A. H.: Ambient Gas-Particle Partitioning of Tracers for Biogenic Oxidation,
848     Environ. Sci. Tech., 50, 9952-9962, 10.1021/acs.est.6b01674, 2016.
849 Jaakkola, E., Gärtner, A., Jönsson, A. M., Ljung, K., Olsson, P. O., and Holst, T.: Spruce bark beetles
850     (Ips typographus) cause up to 700 times higher bark BVOC emission rates compared to healthy
851     Norway spruce (Picea abies), Biogeosciences, 20, 803-826, 10.5194/bg-20-803-2023, 2023.
852 Jacob, D. J., Field, B. D., Jin, E. M., Bey, I., Li, Q., Logan, J. A., Yantosca, R. M., and Singh, H. B.:
853     Atmospheric budget of acetone, J. Geophys. Res. Atmos., 107, ACH 5-1-ACH 5-17,
854     https://doi.org/10.1029/2001JD000694, 2002.
855 Jain, V., Tripathi, N., Tripathi, S. N., Gupta, M., Sahu, L. K., Murari, V., Gaddamidi, S., Shukla, A. K.,
856     and Prevot, A. S. H.: Real-time measurements of non-methane volatile organic compounds in the

central Indo-Gangetic basin, Lucknow, India: source characterisation and their role in O3 and secondary organic aerosol formation, Atmos. Chem. Phys., 23, 3383-3408, 10.5194/acp-23-3383-2023, 2023.

Joó, É., Van Langenhove, H., Šimpraga, M., Steppe, K., Amelynck, C., Schoon, N., Müller, J. F., and Dewulf, J.: Variation in biogenic volatile organic compound emission pattern of Fagus sylvatica L. due to aphid infection, Atmos. Environ., 44, 227-234, https://doi.org/10.1016/j.atmosenv.2009.10.007, 2010.

Jordan, A., Haidacher, S., Hanel, G., Hartungen, E., Mark, L., Seehauser, H., Schottkowsky, R., Sulzer, P., and Mark, T. D.: A high resolution and high sensitivity proton-transfer-reaction time-of-flight mass spectrometer (PTR-TOF-MS), International Journal of Mass Spectrometry, 286, 122-128, 10.1016/j.ijms.2009.07.005, 2009.

Juráň, S., Pallozzi, E., Guidolotti, G., Fares, S., Šigut, L., Calfapietra, C., Alivernini, A., Savi, F., Večeřová, K., Křůmal, K., Večeřa, Z., and Urban, O.: Fluxes of biogenic volatile organic compounds above temperate Norway spruce forest of the Czech Republic, Agricultural and Forest Meteorology, 232, 500-513, https://doi.org/10.1016/j.agrformet.2016.10.005, 2017.

Kari, E., Miettinen, P., Yli-Pirilä, P., Virtanen, A., and Faiola, C. L.: PTR-ToF-MS product ion distributions and humidity-dependence of biogenic volatile organic compounds, International Journal of Mass Spectrometry, 430, 87-97, https://doi.org/10.1016/j.ijms.2018.05.003, 2018.

Kari, E., Faiola, C. L., Isokääntä, S., Miettinen, P., Yli-Pirilä, P., Buchholz, A., Kivimäenpää, M., Mikkonen, S., Holopainen, J. K., and Virtanen, A.: Time-resolved characterization of biotic stress emissions from Scots pines being fed upon by pine weevil by means of PTR-ToF-MS, 2019.

Khare, P., Kumar, N., Kumari, K. M., and Srivastava, S. S.: Atmospheric formic and acetic acids: An overview, Reviews of Geophysics, 37, 227-248, https://doi.org/10.1029/1998RG900005, 1999.

Kleist, E., Mentel, T. F., Andres, S., Bohne, A., Folkers, A., Kiendler-Scharr, A., Rudich, Y., Springer, M., Tillmann, R., and Wildt, J.: Irreversible impacts of heat on the emissions of monoterpenes, sesquiterpenes, phenolic BVOC and green leaf volatiles from several tree species, Biogeosciences, 9, 5111-5123, 10.5194/bg-9-5111-2012, 2012.

Krechmer, J., Lopez-Hilfiker, F., Koss, A., Hutterli, M., Stoermer, C., Deming, B., Kimmel, J., Warneke, C., Holzinger, R., Jayne, J., Worsnop, D., Fuhrer, K., Gonin, M., and de Gouw, J.: Evaluation of a New Reagent-Ion Source and Focusing Ion–Molecule Reactor for Use in Proton-Transfer-Reaction Mass Spectrometry, Analytical Chemistry, 90, 12011-12018, 10.1021/acs.analchem.8b02641, 2018.

Lannuque, V., D'Anna, B., Kostenidou, E., Couvidat, F., Martinez-Valiente, A., Eichler, P., Wisthaler, A., Müller, M., Temime-Roussel, B., Valorso, R., and Sartelet, K.: Gas–particle partitioning of toluene oxidation products: an experimental and modeling study, Atmos. Chem. Phys., 23, 15537-15560, 10.5194/acp-23-15537-2023, 2023.

Lee, B. H., Lopez-Hilfiker, F. D., D'Ambro, E. L., Zhou, P., Boy, M., Petäjä, T., Hao, L., Virtanen, A., and Thornton, J. A.: Semi-volatile and highly oxygenated gaseous and particulate organic compounds observed above a boreal forest canopy, Atmos. Chem. Phys., 18, 11547-11562, 10.5194/acp-18-11547-2018, 2018.

Leglise, J., Müller, M., Piel, F., Otto, T., and Wisthaler, A.: Bulk Organic Aerosol Analysis by Proton-Transfer-Reaction Mass Spectrometry: An Improved Methodology for the Determination of Total Organic Mass, O:C and H:C Elemental Ratios, and the Average Molecular Formula, Anal. Chem., 91, 12619-12624, 10.1021/acs.analchem.9b02949, 2019.

Li, H., Riva, M., Rantala, P., Heikkinen, L., Daellenbach, K., Krechmer, J. E., Flaud, P. M., Worsnop, D., Kulmala, M., Villenave, E., Perraudin, E., Ehn, M., and Bianchi, F.: Terpenes and their oxidation products in the French Landes forest: insights from Vocus PTR-TOF measurements, Atmos. Chem. Phys., 20, 1941-1959, 10.5194/acp-20-1941-2020, 2020.

Li, H., Canagaratna, M. R., Riva, M., Rantala, P., Zhang, Y., Thomas, S., Heikkinen, L., Flaud, P. M., Villenave, E., Perraudin, E., Worsnop, D., Kulmala, M., Ehn, M., and Bianchi, F.: Atmospheric organic vapors in two European pine forests measured by a Vocus PTR-TOF: insights into monoterpene and sesquiterpene oxidation processes, Atmos. Chem. Phys., 21, 4123-4147, 10.5194/acp-21-4123-2021, 2021a.

Li, X. B., Yuan, B., Wang, S., Wang, C., Lan, J., Liu, Z., Song, Y., He, X., Huangfu, Y., Pei, C., Cheng, P., Yang, S., Qi, J., Wu, C., Huang, S., You, Y., Chang, M., Zheng, H., Yang, W., Wang, X., and

Shao, M.: Variations and sources of volatile organic compounds (VOCs) in urban region: insights from measurements on a tall tower, Atmos. Chem. Phys., 22, 10567-10587, 10.5194/acp-22-10567-2022, 2022.

Li, Y., Zhao, J., Wang, Y., Seinfeld, J. H., and Zhang, R.: Multigeneration Production of Secondary Organic Aerosol from Toluene Photooxidation, Environ. Sci. Technol., 55, 8592-8603, 10.1021/acs.est.1c02026, 2021b.

Luo, H., Guo, Y., Shen, H., Huang, D. D., Zhang, Y., and Zhao, D.: Effect of relative humidity on the molecular composition of secondary organic aerosols from α-pinene ozonolysis, Environmental Science: Atmospheres, 10.1039/D3EA00149K, 2024.

Mermet, K., Perraudin, E., Dusanter, S., Sauvage, S., Léonardis, T., Flaud, P.-M., Bsaibes, S., Kammer, J., Michoud, V., Gratien, A., Cirtog, M., Al Ajami, M., Truong, F., Batut, S., Hecquet, C., Doussin, J.-F., Schoemaecker, C., Gros, V., Locoge, N., and Villenave, E.: Atmospheric reactivity of biogenic volatile organic compounds in a maritime pine forest during the LANDEX episode 1 field campaign, Sci. Total Environ., 756, 144129, https://doi.org/10.1016/j.scitotenv.2020.144129, 2021.

Mohr, C., Lopez-Hilfiker, F. D., Yli-Juuti, T., Heitto, A., Lutz, A., Hallquist, M., D'Ambro, E. L., Rissanen, M. P., Hao, L., Schobesberger, S., Kulmala, M., Mauldin III, R. L., Makkonen, U., Sipilä, M., Petäjä, T., and Thornton, J. A.: Ambient observations of dimers from terpene oxidation in the gas phase: Implications for new particle formation and growth, Geophys. Res. Lett., 44, 2958-2966, https://doi.org/10.1002/2017GL072718, 2017.

Muller, M., Eicher, P., D'Anna, B., Tan, W., and Wisthaler, A.: Direct Sampling and Analysis of Atmospheric Particulate Organic Matter by Proton-Transfer-Reaction Mass Spectrometry, Analytical Chemistry, 89, 10889-10897, 10.1021/acs.analchem.7b02582, 2017.

Müller, M., Eichler, P., D'Anna, B., Tan, W., and Wisthaler, A.: Direct Sampling and Analysis of Atmospheric Particulate Organic Matter by Proton-Transfer-Reaction Mass Spectrometry, Anal. Chem., 89, 10889-10897, 10.1021/acs.analchem.7b02582, 2017.

Ng, N. L., Canagaratna, M. R., Jimenez, J. L., Chhabra, P. S., Seinfeld, J. H., and Worsnop, D. R.: Changes in organic aerosol composition with aging inferred from aerosol mass spectra, Atmos. Chem. Phys., 11, 6465-6474, 10.5194/acp-11-6465-2011, 2011.

Ng, N. L., Canagaratna, M. R., Zhang, Q., Jimenez, J. L., Tian, J., Ulbrich, I. M., Kroll, J. H., Docherty, K. S., Chhabra, P. S., Bahreini, R., Murphy, S. M., Seinfeld, J. H., Hildebrandt, L., Donahue, N. M., DeCarlo, P. F., Lanz, V. A., Prevot, A. S. H., Dinar, E., Rudich, Y., and Worsnop, D. R.: Organic aerosol components observed in Northern Hemispheric datasets from Aerosol Mass Spectrometry, Atmos. Chem. Phys., 10, 4625-4641, 10.5194/acp-10-4625-2010, 2010.

Paatero, P. and Tapper, U.: Positive matrix factorization: A non-negative factor model with optimal utilization of error estimates of data values, Environmetrics, 5, 111-126, https://doi.org/10.1002/env.3170050203, 1994.

Pagonis, D., Sekimoto, K., and de Gouw, J.: A Library of Proton-Transfer Reactions of H3O+ Ions Used for Trace Gas Detection, Journal of the American Society for Mass Spectrometry, 30, 1330-1335, 10.1007/s13361-019-02209-3, 2019.

Papurello, D., Soukoulis, C., Schuhfried, E., Cappellin, L., Gasperi, F., Silvestri, S., Santarelli, M., and Biasioli, F.: Monitoring of volatile compound emissions during dry anaerobic digestion of the Organic Fraction of Municipal Solid Waste by Proton Transfer Reaction Time-of-Flight Mass Spectrometry, Bioresource Technology, 126, 254-265, https://doi.org/10.1016/j.biortech.2012.09.033, 2012.

Peng, Y., Wang, H., Gao, Y., Jing, S., Zhu, S., Huang, D., Hao, P., Lou, S., Cheng, T., Huang, C., and Zhang, X.: Real-time measurement of phase partitioning of organic compounds using a proton-transfer-reaction time-of-flight mass spectrometer coupled to a CHARON inlet, Atmos. Meas. Tech., 16, 15-28, 10.5194/amt-16-15-2023, 2023.

Peñuelas, J. and Staudt, M.: BVOCs and global change, Trends Plant Sci., 15, 133-144, 2010.

Pernov, J. B., Bossi, R., Lebourgeois, T., Nøjgaard, J. K., Holzinger, R., Hjorth, J. L., and Skov, H.: Atmospheric VOC measurements at a High Arctic site: characteristics and source apportionment, Atmos. Chem. Phys., 21, 2895-2916, 10.5194/acp-21-2895-2021, 2021.

Peron, A., Kaser, L., Fitzky, A. C., Graus, M., Halbwirth, H., Greiner, J., Wohlfahrt, G., Rewald, B., Sandén, H., and Karl, T.: Combined effects of ozone and drought stress on the emission of biogenic

volatile organic compounds from Quercus robur L, Biogeosciences, 18, 535-556, 10.5194/bg-18-535-2021, 2021.

Piel, F., Müller, M., Winkler, K., Skytte af Sätra, J., and Wisthaler, A.: Introducing the extended volatility range proton-transfer-reaction mass spectrometer (EVR PTR-MS), Atmos. Meas. Tech., 14, 1355-1363, 10.5194/amt-14-1355-2021, 2021.

Rasmussen, R. A. and Went, F.: Volatile organic material of plant origin in the atmosphere, Proc. Natl. Acad. Sci. U.S.A., 53, 215-220, 1965.

Salazar Gómez, J. I., Lohmann, H., and Krassowski, J.: Determination of volatile organic compounds from biowaste and co-fermentation biogas plants by single-sorbent adsorption, Chemosphere, 153, 48-57, https://doi.org/10.1016/j.chemosphere.2016.02.128, 2016.

Scheftelowitz, M., Becker, R., and Thrän, D.: Improved power provision from biomass: A retrospective on the impacts of German energy policy, Biomass and Bioenergy, 111, 1-12, https://doi.org/10.1016/j.biombioe.2018.01.010, 2018.

Shrivastava, M., Cappa, C. D., Fan, J., Goldstein, A. H., Guenther, A. B., Jimenez, J. L., Kuang, C., Laskin, A., Martin, S. T., Ng, N. L., Petaja, T., Pierce, J. R., Rasch, P. J., Roldin, P., Seinfeld, J. H., Shilling, J., Smith, J. N., Thornton, J. A., Volkamer, R., Wang, J., Worsnop, D. R., Zaveri, R. A., Zelenyuk, A., and Zhang, Q.: Recent advances in understanding secondary organic aerosol: Implications for global climate forcing, Reviews of Geophysics, 55, 509-559, https://doi.org/10.1002/2016RG000540, 2017.

Sindelarova, K., Granier, C., Bouarar, I., Guenther, A., Tilmes, S., Stavrakou, T., Müller, J. F., Kuhn, U., Stefani, P., and Knorr, W.: Global data set of biogenic VOC emissions calculated by the MEGAN model over the last 30 years, Atmos. Chem. Phys., 14, 9317-9341, 10.5194/acp-14-9317-2014, 2014.

Smiatek, G. and Steinbrecher, R.: Temporal and spatial variation of forest VOC emissions in Germany in the decade 1994–2003, Atmos. Environ., 40, 166-177, https://doi.org/10.1016/j.atmosenv.2005.11.071, 2006.

Song, J., Saathoff, H., Jiang, F., Gao, L., Zhang, H., and Leisner, T.: Sources of organic gases and aerosol particles and their roles in nighttime particle growth at a rural forested site in southwest Germany, Atmos. Chem. Phys., 24, 6699-6717, 10.5194/acp-24-6699-2024, 2024.

Song, J., Saathoff, H., Gao, L., Gebhardt, R., Jiang, F., Vallon, M., Bauer, J., Norra, S., and Leisner, T.: Variations of PM2.5 sources in the context of meteorology and seasonality at an urban street canyon in Southwest Germany, Atmos. Environ., 119147, https://doi.org/10.1016/j.atmosenv.2022.119147, 2022.

Surdu, M., Lamkaddam, H., Wang, D. S., Bell, D. M., Xiao, M., Lee, C. P., Li, D., Caudillo, L., Marie, G., Scholz, W., Wang, M., Lopez, B., Piedehierro, A. A., Ataei, F., Baalbaki, R., Bertozzi, B., Bogert, P., Brasseur, Z., Dada, L., Duplissy, J., Finkenzeller, H., He, X.-C., Höhler, K., Korhonen, K., Krechmer, J. E., Lehtipalo, K., Mahfouz, N. G. A., Manninen, H. E., Marten, R., Massabò, D., Mauldin, R., Petäjä, T., Pfeifer, J., Philippov, M., Rörup, B., Simon, M., Shen, J., Umo, N. S., Vogel, F., Weber, S. K., Zauner-Wieczorek, M., Volkamer, R., Saathoff, H., Möhler, O., Kirkby, J., Worsnop, D. R., Kulmala, M., Stratmann, F., Hansel, A., Curtius, J., Welti, A., Riva, M., Donahue, N. M., Baltensperger, U., and El Haddad, I.: Molecular Understanding of the Enhancement in Organic Aerosol Mass at High Relative Humidity, Environ. Sci. Technol., 57, 2297-2309, 10.1021/acs.est.2c04587, 2023.

Tani, A., Hayward, S., and Hewitt, C. N.: Measurement of monoterpenes and related compounds by proton transfer reaction-mass spectrometry (PTR-MS), International Journal of Mass Spectrometry, 223-224, 561-578, https://doi.org/10.1016/S1387-3806(02)00880-1, 2003.

Teskey, R., Wertin, T., Bauweraerts, I., Ameye, M., McGuire, M. A., and Steppe, K.: Responses of tree species to heat waves and extreme heat events, Plant, Cell & Environment, 38, 1699-1712, https://doi.org/10.1111/pce.12417, 2015.

Tillmann, R., Hallquist, M., Jonsson, Å. M., Kiendler-Scharr, A., Saathoff, H., Iinuma, Y., and Mentel, T. F.: Influence of relative humidity and temperature on the production of pinonaldehyde and OH radicals from the ozonolysis of α-pinene, Atmos. Chem. Phys., 10, 7057-7072, 10.5194/acp-10-7057-2010, 2010.

1019 Trainer, M., Williams, E. J., Parrish, D. D., Buhr, M. P., Allwine, E. J., Westberg, H. H., Fehsenfeld, F.
1020      C., and Liu, S. C.: Models and observations of the impact of natural hydrocarbons on rural ozone,
1021      Nature, 329, 705-707, 10.1038/329705a0, 1987.
1022 van Meeningen, Y., Schurgers, G., Rinnan, R., and Holst, T.: Isoprenoid emission response to changing
1023      light conditions of English oak, European beech and Norway spruce, Biogeosciences, 14, 4045-
1024      4060, 10.5194/bg-14-4045-2017, 2017.
1025 Vermeuel, M. P., Novak, G. A., Kilgour, D. B., Claflin, M. S., Lerner, B. M., Trowbridge, A. M., Thom,
1026      J., Cleary, P. A., Desai, A. R., and Bertram, T. H.: Observations of biogenic volatile organic
1027      compounds over a mixed temperate forest during the summer to autumn transition, Atmos. Chem.
1028      Phys., 23, 4123-4148, 10.5194/acp-23-4123-2023, 2023.
1029 Vestenius, M., Hopke, P. K., Lehtipalo, K., Petäjä, T., Hakola, H., and Hellén, H.: Assessing volatile
1030      organic compound sources in a boreal forest using positive matrix factorization (PMF), Atmos.
1031      Environ., 259, 118503, https://doi.org/10.1016/j.atmosenv.2021.118503, 2021.
1032 von Hessberg, C., von Hessberg, P., Pöschl, U., Bilde, M., Nielsen, O. J., and Moortgat, G. K.:
1033      Temperature and humidity dependence of secondary organic aerosol yield from the ozonolysis of β-
1034      pinene, Atmos. Chem. Phys., 9, 3583-3599, 10.5194/acp-9-3583-2009, 2009.
1035 Wang, L., Slowik, J. G., Tripathi, N., Bhattu, D., Rai, P., Kumar, V., Vats, P., Satish, R., Baltensperger,
1036      U., Ganguly, D., Rastogi, N., Sahu, L. K., Tripathi, S. N., and Prévôt, A. S. H.: Source
1037      characterization of volatile organic compounds measured by proton-transfer-reaction time-of-flight
1038      mass spectrometers in Delhi, India, Atmos. Chem. Phys., 20, 9753-9770, 10.5194/acp-20-9753-
1039      2020, 2020.
1040 Weber, J., Archer-Nicholls, S., Abraham, N. L., Shin, Y. M., Griffiths, P., Grosvenor, D. P., Scott, C.
1041      E., and Archibald, A. T.: Chemistry-driven changes strongly influence climate forcing from
1042      vegetation emissions, Nature Communications, 13, 7202, 10.1038/s41467-022-34944-9, 2022.
1043 Wennberg, P. O., Bates, K. H., Crounse, J. D., Dodson, L. G., McVay, R. C., Mertens, L. A., Nguyen,
1044      T. B., Praske, E., Schwantes, R. H., Smarte, M. D., St Clair, J. M., Teng, A. P., Zhang, X., and
1045      Seinfeld, J. H.: Gas-Phase Reactions of Isoprene and Its Major Oxidation Products, Chem Rev, 118,
1046      3337-3390, 10.1021/acs.chemrev.7b00439, 2018.
1047 Wu, R., Pan, S., Li, Y., and Wang, L.: Atmospheric Oxidation Mechanism of Toluene, The Journal of
1048      Physical Chemistry A, 118, 4533-4547, 10.1021/jp500077f, 2014.
1049 Yáñez-Serrano, A. M., Bach, A., Bartolomé-Catalá, D., Matthaios, V., Seco, R., Llusià, J., Filella, I.,
1050      and Peñuelas, J.: Dynamics of volatile organic compounds in a western Mediterranean oak forest,
1051      Atmos. Environ., 257, 118447, https://doi.org/10.1016/j.atmosenv.2021.118447, 2021.
1052 Yáñez-Serrano, A. M., Bourtsoukidis, E., Alves, E. G., Bauwens, M., Stavrakou, T., Llusià, J., Filella,
1053      I., Guenther, A., Williams, J., Artaxo, P., Sindelarova, K., Doubalova, J., Kesselmeier, J., and
1054      Peñuelas, J.: Amazonian biogenic volatile organic compounds under global change, Global Change
1055      Biology, 26, 4722-4751, https://doi.org/10.1111/gcb.15185, 2020.
1056 Yatavelli, R. L. N., Stark, H., Thompson, S. L., Kimmel, J. R., Cubison, M. J., Day, D. A., Campuzano-
1057      Jost, P., Palm, B. B., Hodzic, A., Thornton, J. A., Jayne, J. T., Worsnop, D. R., and Jimenez, J. L.:
1058      Semicontinuous measurements of gas–particle partitioning of organic acids in a ponderosa pine
1059      forest using a MOVI-HRToF-CIMS, Atmos. Chem. Phys., 14, 1527-1546, 10.5194/acp-14-1527-
1060      2014, 2014.
1061 Zaytsev, A., Koss, A. R., Breitenlechner, M., Krechmer, J. E., Nihill, K. J., Lim, C. Y., Rowe, J. C.,
1062      Cox, J. L., Moss, J., Roscioli, J. R., Canagaratna, M. R., Worsnop, D. R., Kroll, J. H., and Keutsch,
1063      F. N.: Mechanistic study of the formation of ring-retaining and ring-opening products from the
1064      oxidation of aromatic compounds under urban atmospheric conditions, Atmos. Chem. Phys., 19,
1065      15117-15129, 10.5194/acp-19-15117-2019, 2019.
1066 Zhang, X., McVay, R. C., Huang, D. D., Dalleska, N. F., Aumont, B., Flagan, R. C., and Seinfeld, J. H.:
1067      Formation and evolution of molecular products in α-pinene secondary organic aerosol,
1068      Proceedings of the National Academy of Sciences, 112, 14168-14173,
1069      doi:10.1073/pnas.1517742112, 2015.

1070

1071
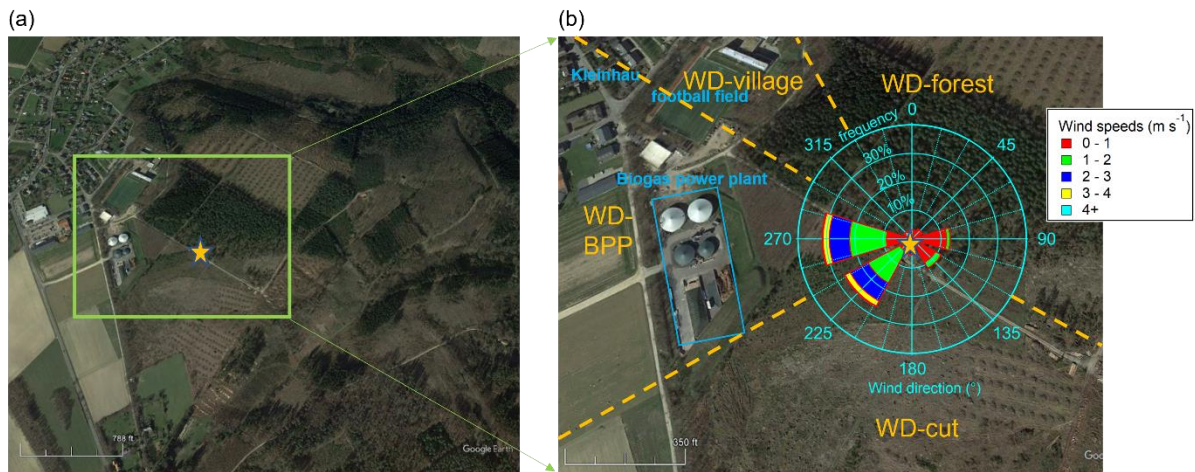
**Figure 1.** (a) Location of the sampling site (orange star) (©Google Earth); (b) a close look at sampling site with the centered wind rose for the entire measurement period. The orange dash lines are shown for distinguishing different sectors of wind direction (WD). The WD-forest of 0-120° is influenced by an intact forest area, the WD-cut of 120-240° is influenced by a clear-cut area, the WD-BPP of 240-300° is influenced by a biogas power plant (blue rectangle) and the WD-village of 300-330° is influenced by the residential areas of Kleinhau.
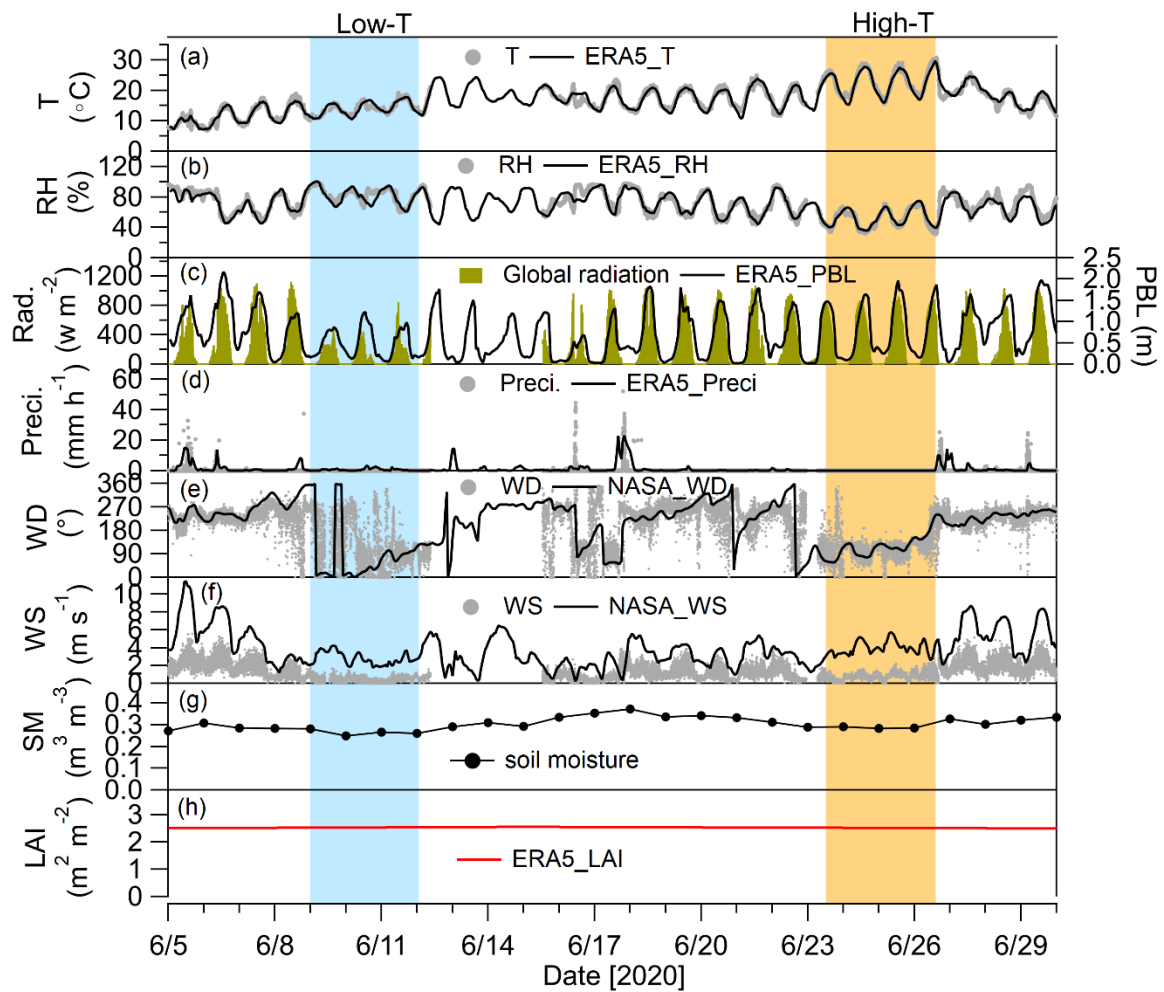
1080

**Figure 2.** (a-f) Time series of meteorological data measured at the sampling site with hourly data of temperature (T), relative humidity (RH), precipitation (Preci.) and planetary boundary layer (PBL) height obtained from ERA5 reanalysis (Hersbach et al., 2020) and hourly data of wind direction and speed (WD and WS) obtained from NASA Power Data Access Viewer (power.larc.nasa.gov); (g) daily soil moisture (SM) measured by a cosmic ray neutron sensor which was located ~ 150 m southwest of the sampling site; and (h) leaf area index (LAI) obtained from ERA5 reanalysis. The blue and yellow shaded areas mark the low-T and high-T episodes.
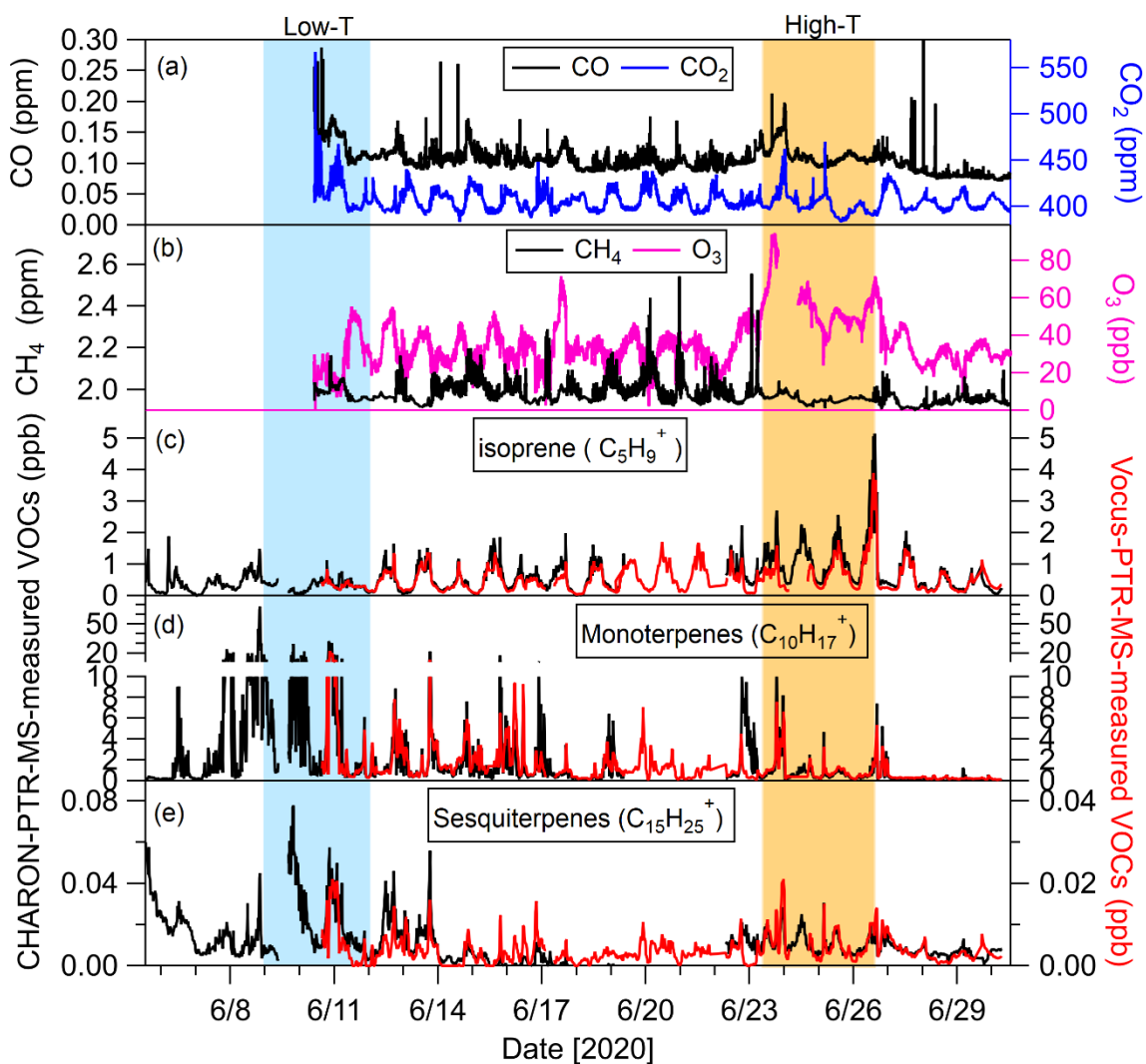
1089

**Figure 3.** Time series of gas concentrations: (a) CO and $CO_2$; (b) $CH_4$ and $O_3$; (c-e) isoprene, monoterpenes, sesquiterpenes measured by the CHARON-PTR-MS (black lines) and Vocus-PTR-MS (red lines) respectively. The blue and yellow shaded areas mark the low-T and high-T episodes.
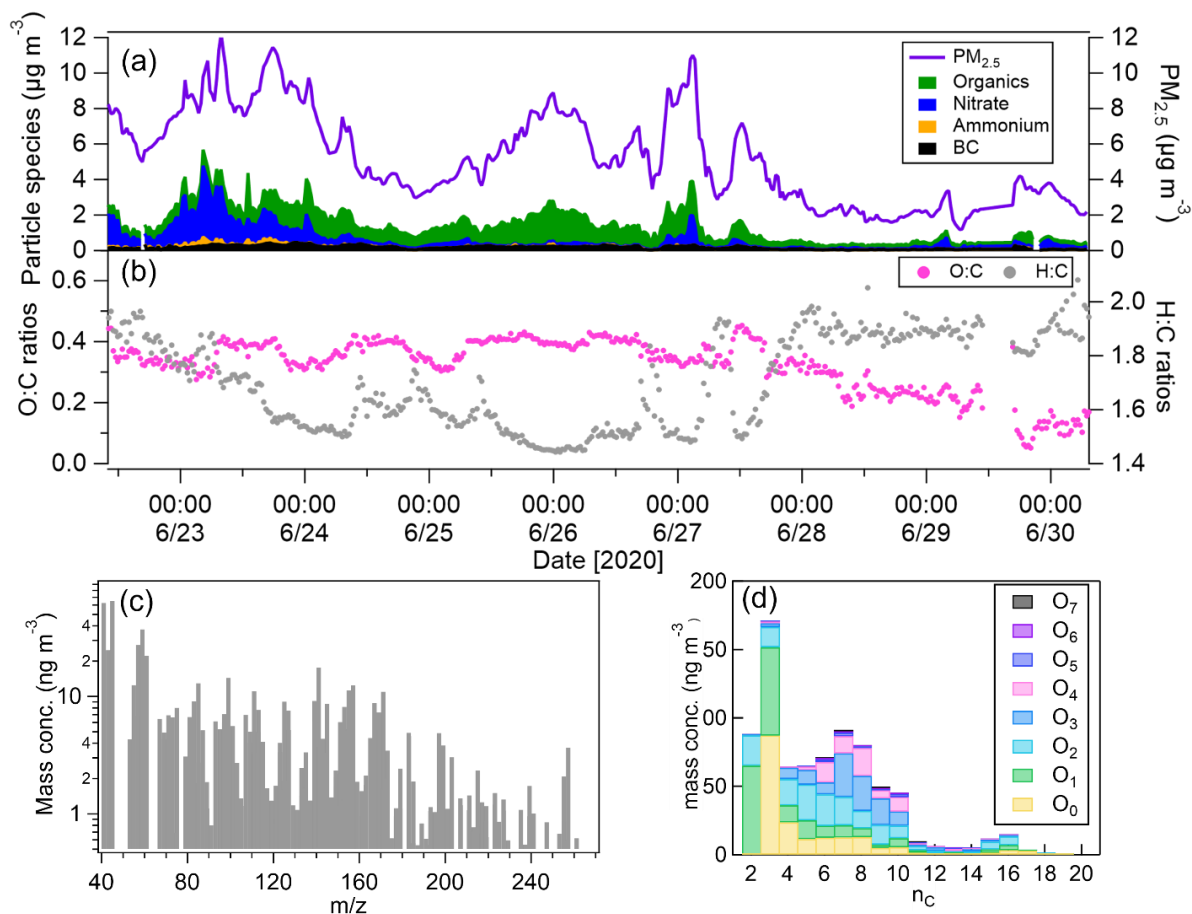
1094

**Figure 4.** Time series of (a) mass concentrations of $PM_{2.5}$, BC and semi-volatile particle species (organics, nitrate and ammonium) measured by the CHARON-PTR-ToF-MS simultaneously available during $22^{nd}$-$30^{th}$ June; (b) oxygen to carbon (O:C) and hydrogen to carbon (H:C) ratios of organics. (c) average mass spectrum of organics; (d) mass distributions of organics associated with $C_xH_yO_{0-7}^+$ resolved by the carbon and oxygen numbers ($n_C$ and $n_O$).
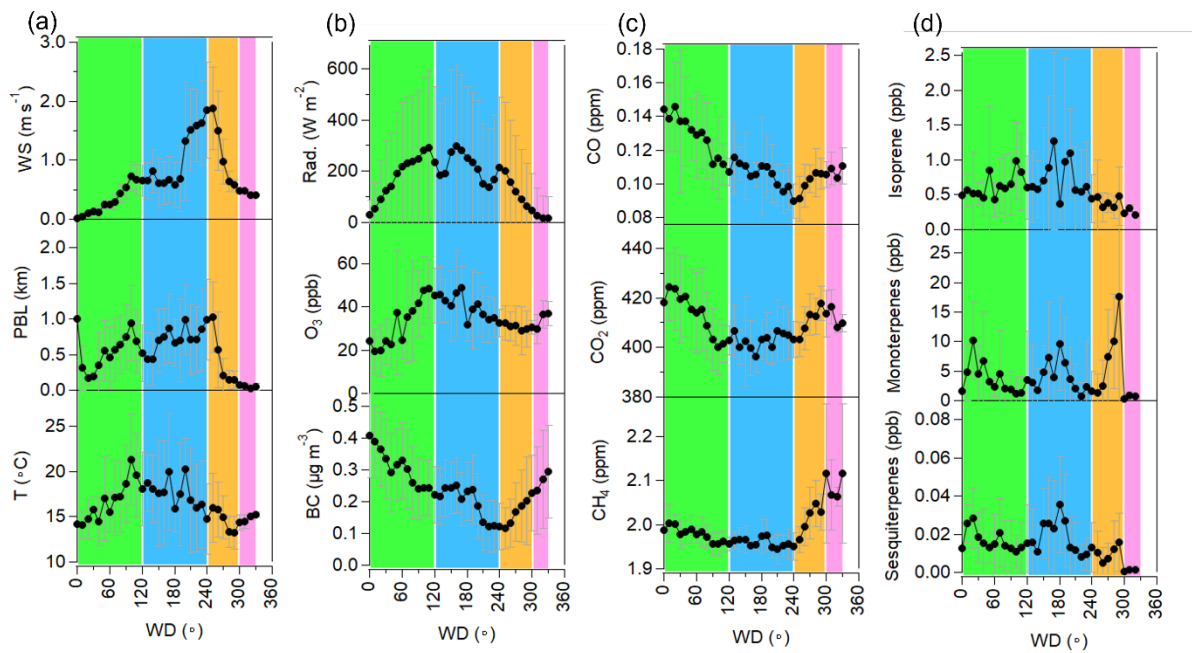
1100

**Figure 5.** Variations of (a) wind speed (WS), planetary boundary layer (PBL) and ambient temperature; (b) global radiation, $O_3$ and BC mass concentrations; (c) mixing ratios of CO, $CO_2$ and $CH_4$ and (d) mixing ratios of isoprene, monoterpenes and sesquiterpenes as a function of wind direction (WD). The black dots and whiskers represent the mean values and standard deviations in each WD bin of 10°. Data within the WD1 of 0-120° is influenced by an intact forest area (light green), the WD2 of 120-240° is influenced by a clear-cut area (light blue), the WD3 of 240-300° is influenced by a biogas power plant (yellow) and the WD4 of 300-330° is influenced by the village (pink).
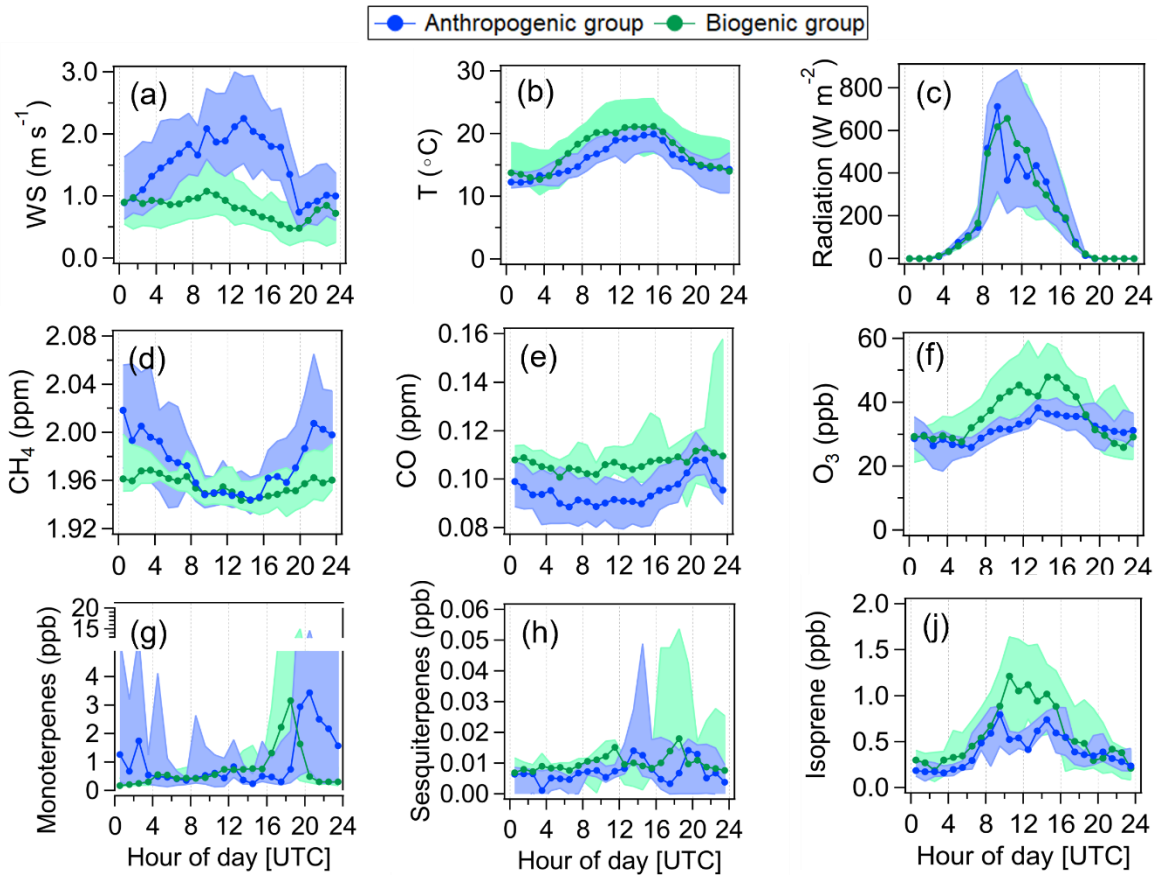
**Figure 6.** Diurnal variations of (a-c) wind speeds, ambient temperature and global radiation; (d-f) $CH_4$, CO and $O_3$; (g-j) monoterpenes, sesquiterpenes and isoprene. The blue and green markers represent the median values for the anthropogenic-group and biogenic-group, which were calculated from the data within the sectors of WD-forest and WD-cut, and WD-BPP and WD-village, respectively. The shaded areas represent the 25th and 75th percentiles.
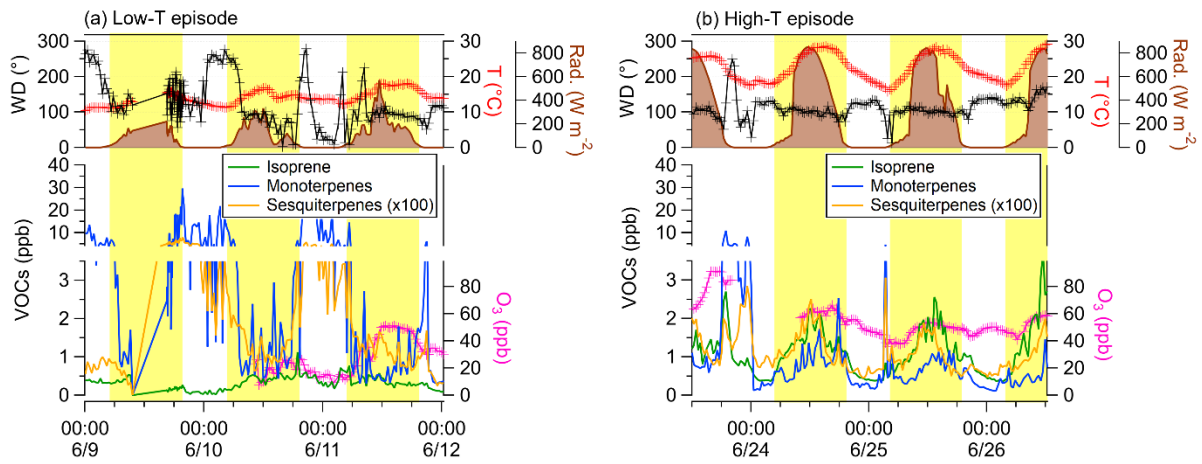
1117 **Figure 7.** Time series of wind direction, ambient temperature, global radiation, isoprene,

1118 monoterpenes, sesquiterpenes and $O_3$ during the low-T episode (a) and high-T episode (b). The

1119 yellow shaded areas mark the daytime from 4:00-20:00 UTC.

1120
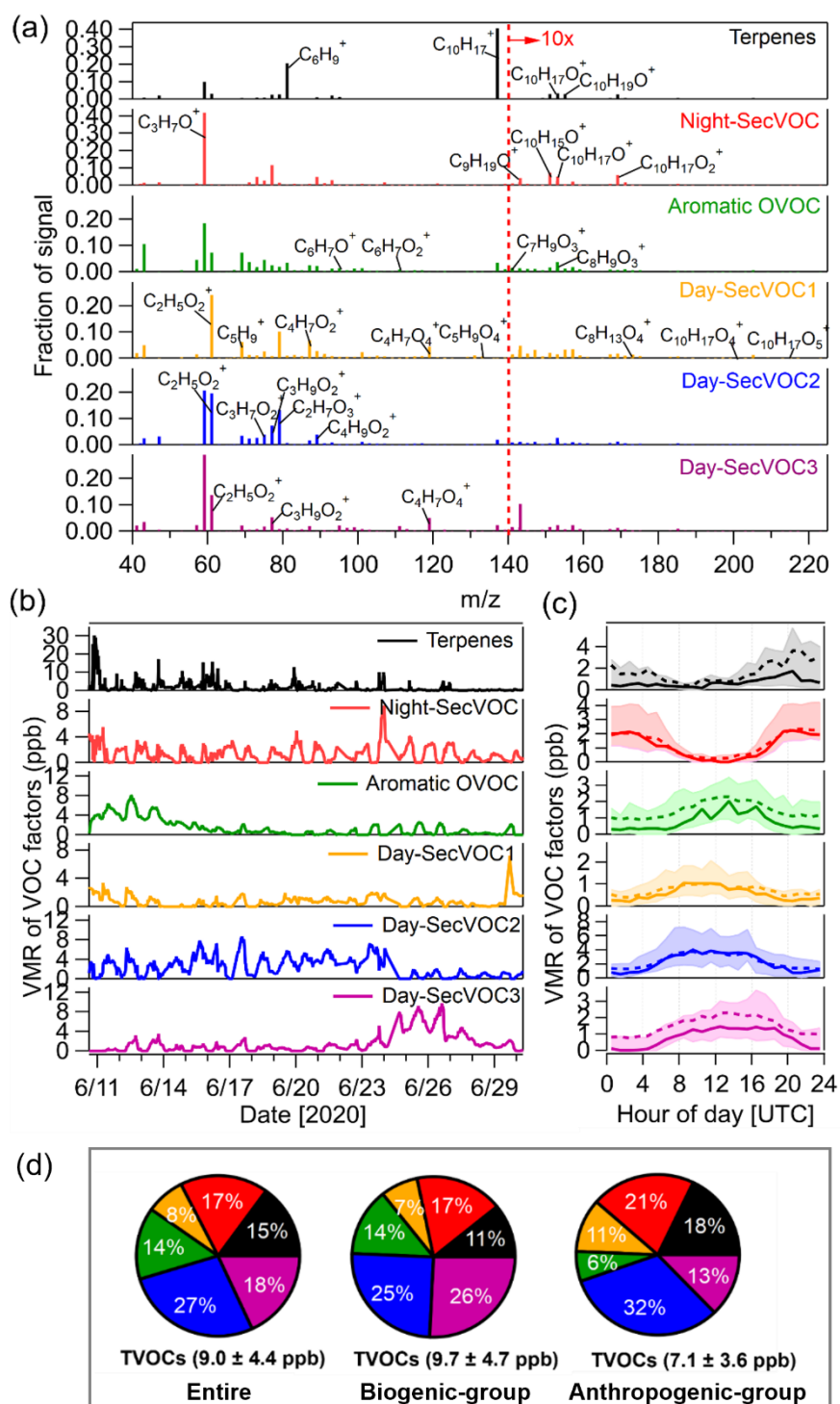
**Figure 8.** (a) Factor profiles of six VOC factors resolved from the PMF analysis of Vocus-PTR-ToF-MS data. The fraction of signal at high mass range ($m/z$ 140-230) is scaled by a factor of 10; (b) time series of six VOC factors; (c) diurnal variations of six VOC factors during the entire measurement campaign. The solid and dash lines represent median and mean values respectively and the shaded areas represent the $25^{th}$ and $75^{th}$ percentiles. (d) Average contributions of six VOC factors to TVOCs for the entire measurement campaign and the biogenic-group and anthropogenic-group.
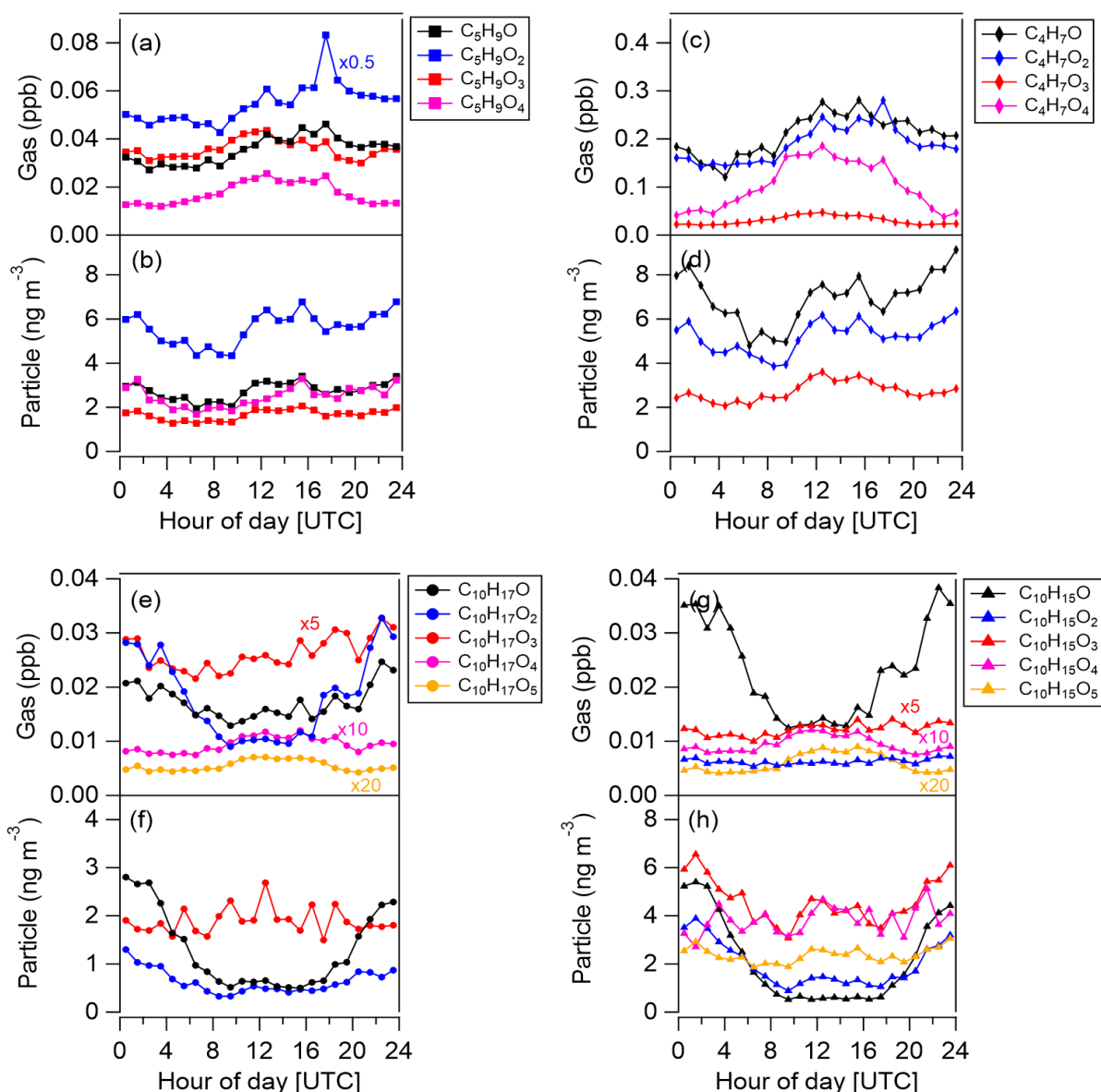
1129

**Figure 9.** Diurnal variations of (a-d) concentrations of isoprene oxidation products ($C_5H_9O_{1-4}^+$ and $C_4H_7O_{1-4}^+$) in gas and particle phases; (e-h) concentrations of monoterpene oxidation products ($C_{10}H_{17}O_{1-5}^+$ and $C_{10}H_{15}O_{1-5}^+$) in gas and particle phases calculated for the measurement period of 22$^{nd}$-30$^{th}$ of June. Gas- and particle-phase data were taken from the Vocus-PTR-ToF-MS and CHARON-PTR-ToF-MS measurements, respectively. The higher-oxidized particle-phase products from isoprene ($C_4H_7O_4^+$) and monoterpenes ($C_{10}H_{17}O_{4-5}^+$) cannot be detected by the CHARON-PTR-ToF-MS.
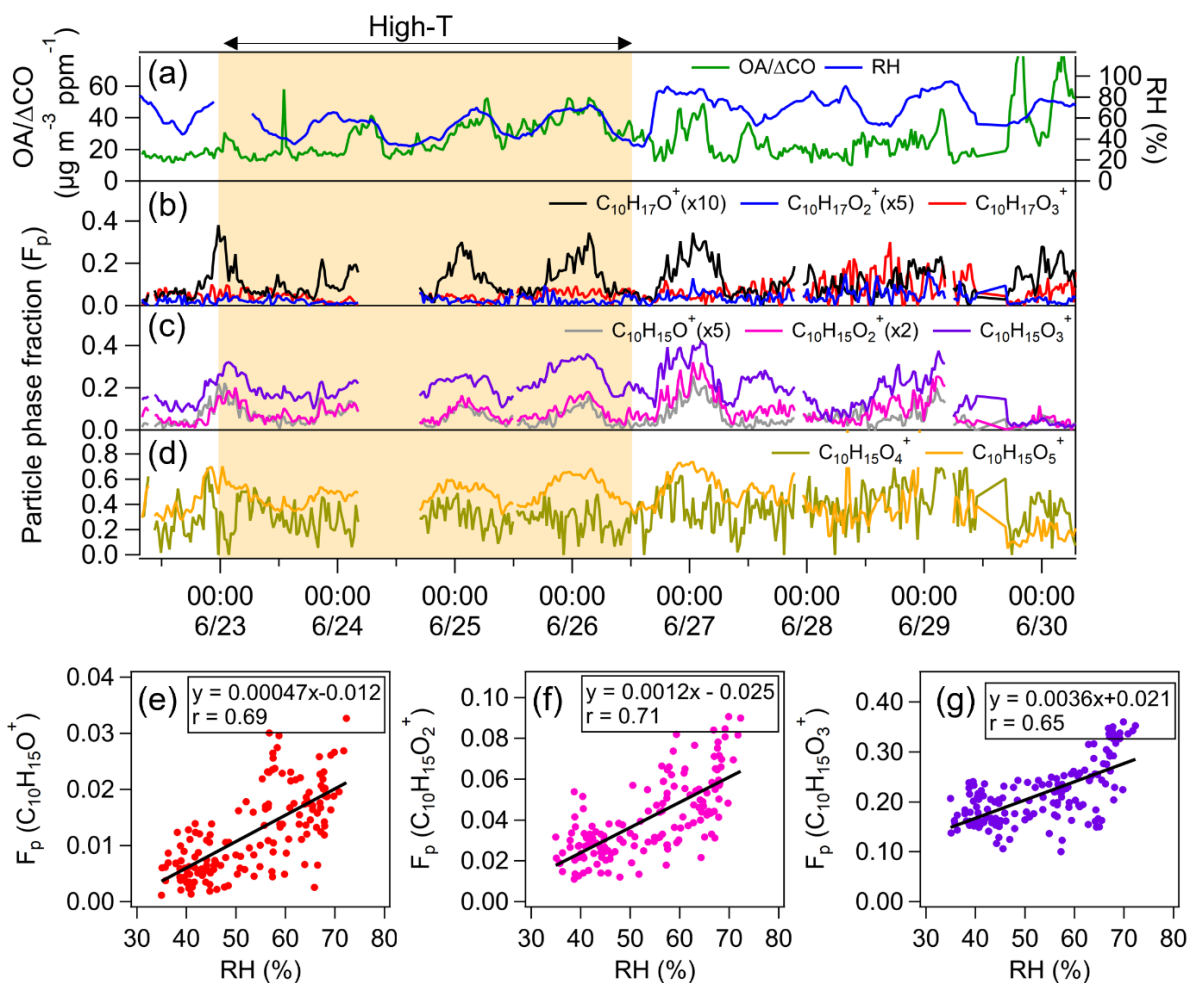
**Figure 10.** Time series of (a) OA/ΔCO and relative humidity (RH); (b-d) particle phase fraction of monoterpene oxidation products ($C_{10}H_{17}O_{1-3}^+$ and $C_{10}H_{15}O_{1-5}^+$) from $22^{nd}$-$30^{th}$ of June. The yellow shaded area marks the high-T episode. (e-f) Correlations of the time series of particle phase fraction of $C_{10}H_{15}O_{1-3}^+$ with RH during high-T episode.